Rhodium and Iridium Complexes Bearing "Capping Arene" Ligands: Synthesis and Characterization

Shunyan Gu[†], Charles B. Musgrave III[‡], Zoë M. Gehman[†], Ke Zhang[†], Diane A. Dickie[†], William A. Goddard III,[‡*] and T. Brent Gunnoe[†*]

Department of Chemistry, University of Virginia, Charlottesville, Virginia 22904, United States

Materials and Process Simulation Center, California Institute of Technology, Pasadena, California 91125, United States

ABSTRACT

A series of olefin coordinated Rh^{I} and Ir^{I} complexes bearing "capping arene" ligands (5-^{X}FP and 6-^{X}FP, see below) of the general formula (FP)M(olefin)X, [(FP)M(olefin)$_2$][M(olefin)$_2$X$_2$] or [(FP)M(olefin)$_2$]BF_4 (FP = "capping arene" ligands, X = halide or pseudohalide, olefin = ethylene, cyclooctene, (olefin)$_2$ = $(C_2H_4)_2$ or cyclooctadiene) were synthesized and characterized. Single crystal X-ray diffraction studies revealed structural differences that are a function of the identity of the capping arene ligand and the metal. For 5-^{X}FP ligands (5-^{X}FP = 1,2-bis(*N*-7-azaindolyl)-benzene and derivatives with substituents on the arene moiety), the coordination to both Rh and Ir gives rise to complexes that are best described as 16-electron and square planar. For 6-^{X}FP ligands (6-^{X}FP = 8,8'-(1,2-phenylene)diquinoline and derivatives with substituents on the arene moiety), the structures of Rh and Ir complexes are better considered as 18-electron and trigonal bipyramidal due to an η^2-C,C interaction between the metal center and the arene group of the capping arene ligand. Variable temperature ^{1}H NMR spectroscopy studies of ethylene rotation demonstrated that the Ir complexes possess a higher

activation barrier to rotation than Rh complexes, and the 6-^{X}FP complexes tend to give ethylene higher rotational barriers than 5-^{X}FP complexes for complexes of the type (FP)Rh(η^2-C_2H_4)Cl. DFT calculations are consistent with enhanced Rh-to-ethylene π-back-donation for Rh complexes ligated by the 6-^{X}FP ligands compared to the 5-^{X}FP ligands.

INTRODUCTION

Ligand-controlled reactivity is a hallmark of molecular inorganic and organometallic chemistry. Ligand-influenced reactivity is often complicated and can be affected by various factors including, but not limited to, 1) control of the number, types and strength of various types of metal-ligand bonding interactions (including σ-, π- and δ-bonding), 2) control based on the size of the ligand, and 3) control of the energetics of reactions that give changes in metal oxidation state, which can result in geometry and/or coordination number changes.

Recently, our group reported the isolation and study of a series of "capping arene" ligated Rh complexes (Scheme 1).[1-5] We were drawn to the capping arene ligand motif based on the possibility of modulating the metal/arene interaction through ligand structure and, hence, influencing metal-mediated reactivity, especially for redox reactions that involve substantial changes in the metal geometry. For example, a potential leverage point of the capping arene ligand structure is the ability to control the distance between the metal center and the arene group by adjusting the N–A backbone (see Scheme 1) between the coordination atom and the arene moiety. Also, the electronic properties of capping arene ligands can be modified by substituents on the arene (X and Y in Scheme 1). For the 6-^{X}FP Rh complexes (see Scheme 1 for explanation of ligand abbreviations), we found that the ligand structure gives rise to a dihapto interaction between the Rh center and the arene.[1, 2, 4] In contrast, no such interaction was observed for Rh 5-^{X}FP complexes.[1, 2, 4] Thus, the structures of these Rh complexes are consistent with our proposal that the properties of 5-^{X}FP and 6-^{X}FP ligands, specifically their interactions with metal centers, can be modulated. Based on these results, upon coordination to d^8 metals we anticipate that 5-^{X}FP ligands will promote reactivity that is consistent with 16-electron complexes while

6-^{X}FP ligands are more likely to donate two additional electrons, forming 18-electron complexes, through the arene group. That is, 6-^{X}FP ligands are more likely to serve as tridentate ligands through a combination of κ^2-*N,N* and η^2-*C,C* binding modes.

Scheme 1. The design of "capping arene" ligands including 5-^{X}FP and 6-^{X}FP ligands in this work. The dashed line in the 6-^{X}FP structure (bottom right) shows the η^2 coordination between the metal center and arene moiety.[5]

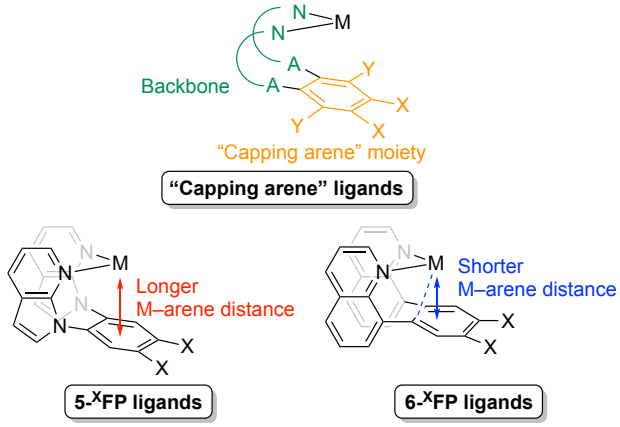

Metal olefin complexes are important intermediates in a variety of catalytic reactions, such as olefin polymerization, olefin hydrogenation, olefin metathesis and olefin oxidation.[6-12] Upon coordination of an olefin to a transition metal, the π bonding orbital of the olefin donates electrons (σ donation) to the metal center through an η^2 interaction, and for d^n metal centers (n > 0), the metal can π-back-donate into the π* antibonding orbital of the olefin.[13, 14] Olefin coordinated Rh and Ir complexes have been of interest due to their potential involvement in catalytic reactions such as olefin polymerization, olefin hydroamination, olefin oxidation, and catalytic olefin C–H functionalization.[3, 15-32]

Herein, we report the synthesis and characterization of a series of Rh^{I} and Ir^{I} η^2-olefin complexes bearing 5-^{X}FP and 6-^{X}FP ligands. We hypothesized that the difference of 5-^{X}FP and 6-^{X}FP ligands in the η^2 interaction will impact metal-ethylene bonding. Through NMR experiments, X-ray crystallography and

computational modeling, our studies revealed that (6-^{X}FP)M(C_2H_4)Cl complexes have a higher rotational barrier for ethylene rotation and longer ethylene C=C bond lengths than (5-^{X}FP)M(C_2H_4)Cl complexes, which we propose is due to the stronger donor ability of 6-^{X}FP ligands compared to 5-^{X}FP ligands.

RESULTS AND DISCUSSION

Synthesis and Characterization of Rhodium Complexes. Seven proligands, 5-FP (1,2-bis(*N*-7-azaindolyl)-benzene, **1**), 5-^{NP}FP (2,3-bis(*N*-7-azaindolyl)-naphthalene, **2**), 5-^{Me}FP (4,5-bis(*N*-7-azaindolyl)-1,2-dimethylbenzene, **3**), 6-FP (8,8'-(1,2-phenylene)diquinoline, **4**), 6-^{NP}FP (8,8'-(1,2-naphthalene)diquinoline, **5**), 6-^{Me}FP (8,8'-(1,2-(4,5-dimethylphenylene))diquinoline, **6**) and 6-^{F}FP (8,8'-(1,2-(4,5-difluorophenylene))diquinoline, **7**), were selected for this study (Scheme 2). The compound 5-^{Me}FP (4,5-bis(*N*-7-azaindolyl)-1,2-dimethylbenzene, **3**) was synthesized by a Cu-catalyzed Ullmann reaction using 2.4 equiv. of 7-azaindole and 1 equiv. 4,5-dibromo-1,2-dimethylbenzene as the starting materials (Scheme 3).[3, 33] Other proligands, 5-FP (**1**), 5-^{NP}FP (**2**), 6-FP (**4**), 6-^{NP}FP (**5**), 6-^{Me}FP (**6**) and 6-^{F}FP (**7**), as well as some of the corresponding Rh complexes, (5-FP)Rh(C_2H_4)Cl (**1a**), (5-^{NP}FP)Rh(C_2H_4)Cl (**2a**), (6-FP)Rh(C_2H_4)Cl (**4a**) and (6-^{NP}FP)Rh(C_2H_4)Cl (**5a**) were synthesized following published procedures.[1-3, 33, 34] The new Rh complexes, (5-^{Me}FP)Rh(C_2H_4)Cl (**3a**) and (6-^{Me}FP)Rh(C_2H_4)Cl (**6a**), were synthesized using a method similar to the synthesis of **1a**.[5]

Scheme 2. Ligands used in this study.

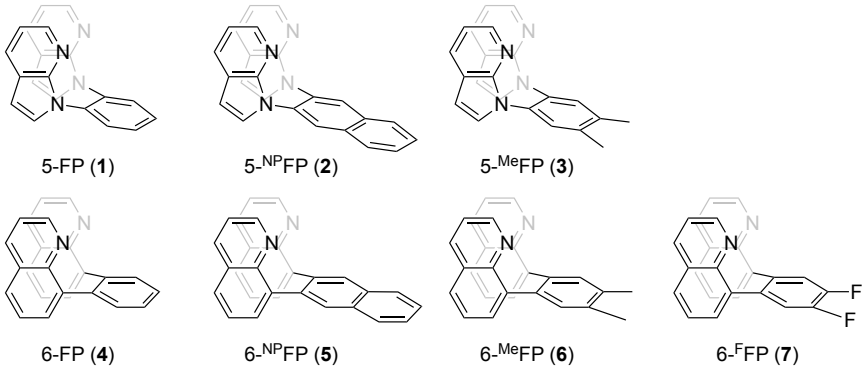

Scheme 3. Synthesis of 5-^{Me}FP (**3**) and (5-^{Me}FP)Rh(C_2H_4)Cl (**3a**).

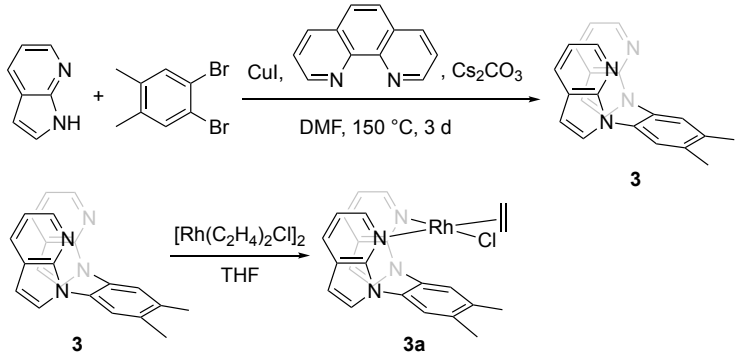

The room temperature ^{1}H NMR spectra of (5-FP)Rh(C_2H_4)Cl (**1a**) and (5-^{NP}FP)Rh(C_2H_4)Cl (**2a**) each show two broad peaks for the coordinated C_2H_4, indicating likely rapid rotation of the C_2H_4 ligand on the ^{1}H NMR time scale (Figure 1). The ethylene peaks of (5-^{Me}FP)Rh(C_2H_4)Cl (**3a**) are broad at room temperature, indicating that a fluxional process, likely ethylene rotation, is occurring. For **3a**, there are two peaks, each with an integration of two protons, but one of them overlaps with the methyl resonances of the arene group. Four broad resonances are observed in the ^{1}H NMR spectra for coordinated C_2H_4 of both (6-FP)Rh(C_2H_4)Cl (**4a**) and (6-^{Me}FP)Rh(C_2H_4)Cl (**6a**), and the ethylene resonances of (6-^{NP}FP)Rh(C_2H_4)Cl (**5a**) appear as four distinct triplets with $^3J_{HH}$ = 10 Hz. Coordinated ethylene resonances in ^{13}C{^{1}H} spectra of **1a**, **2a**, **3a**, **4a** and **6a** appear as broad peaks, while the resonance of

ethylene for **5a** displays a doublet splitting pattern ($^1J_{CRh}$ = 15 Hz).[5] Although quantitative comparisons cannot be made without variable temperature assessments (see below), based on the observations of room temperature ^{1}H and ^{13}C{^{1}H} NMR spectra, the relative activation barriers for C_2H_4 rotation of the six Rh complexes can be estimated as **5a** > **6a** ≈ **4a** > **3a** ≈ **2a** ≈ **1a**.

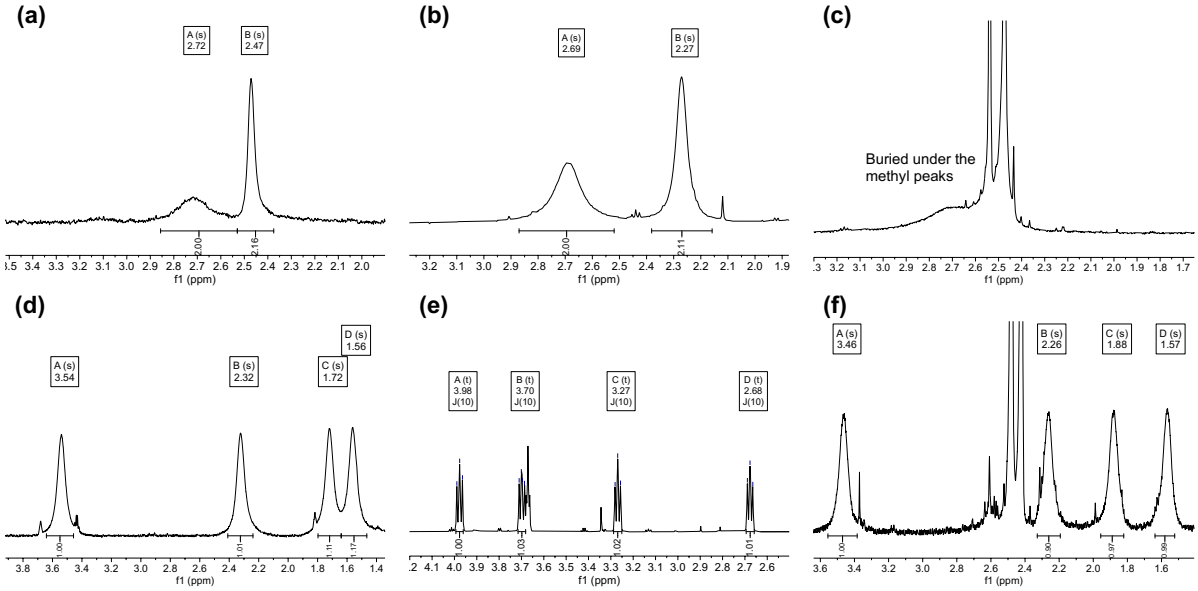

Figure 1. Resonances due to coordinated C_2H_4 in the ^{1}H NMR spectra of complexes **1a**–**6a**. (a) (5-FP)Rh(C_2H_4)Cl (**1a**). (b) (5-^{NP}FP)Rh(C_2H_4)Cl (**2a**). (c) (5-^{Me}FP)Rh(C_2H_4)Cl (**3a**). (d) (6-FP)Rh(C_2H_4)Cl (**4a**). (e) (6-^{NP}FP)Rh(C_2H_4)Cl (**5a**). (f) (6-^{Me}FP)Rh(C_2H_4)Cl (**6a**).[5]

The crystal structure of (6-^{Me}FP)Rh(C_2H_4)Cl (**6a**) (Figure 2) indicates a similar structure to (6-FP)Rh(C_2H_4)Cl (**4a**).[5] The Rh center presents as a trigonal bipyramidal structure, with one N atom and Cl sitting at the axial position. The distances between Rh and the two coordinating carbons on the arene (2.551(10) and 2.558(10) Å, respectively) are similar to that in **4a** (2.578(3) and 2.553(3) Å, respectively).

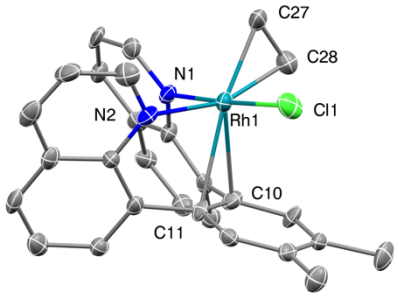

Figure 2. ORTEP of (6-^{Me}FP)Rh(C_2H_4)Cl (**6a**). Ellipsoids are drawn at the 50% probability level, and hydrogen atoms are omitted for clarity. Selected bond lengths for **6a** (Å): Rh–N_1 2.024(8), Rh–N_2 2.196(9), Rh–Cl 2.334(3), Rh–C_{27} 2.066(10), Rh–C_{28} 2.051(10), Rh–C_{10} 2.558(10), Rh–C_{11} 2.551(10), C_{27}–C_{28} 1.396(15), C_{10}–C_{11} 1.412(14).

Synthesis and Characterization of Ir Complexes Bearing 5-^{X}FP Ligands. Mixing 5-FP (**1**) and $[Ir(COE)_2(\mu\text{-}Cl)]_2$ (COE = cyclooctene) in 1:1 ratio (i.e., a 2:1 ratio of Ir atoms and 5-FP) did not result in the formation of (5-FP)Ir(COE)Cl (**1f**). Instead, a new Ir complex with NMR features indicating likely mirror symmetry (e.g., 7 resonances in the aromatic region of the ^{1}H NMR spectrum) is formed, which is inconsistent with the structure of **1f**. Mixing 5-FP and $[Ir(COE)_2(\mu\text{-}Cl)]_2$ in 2:1 molar ratio (i.e., a 1:1 ratio of 5-FP and Ir atoms) produces the same Ir complex along with uncoordinated 5-FP. Thus, the new Ir complex is a result of a 2:1 Ir to ligand ratio. Analysis of single crystals by X-ray diffraction allowed the identification of the complex as [(5-FP)Ir(η^2,η^2-COD)][$IrCl_2$(η^2,η^2-COD)] (**1b**, COD = 1,5-cyclooctadiene, Figure 3a), which is consistent with the NMR spectra (Scheme 4). The formation of **1b** can be explained by Ir-mediated C–H activation of COE, to form COD, and net dihydrogen transfer to another equivalent of COE to give cyclooctane (COA) (Figure S63).[29, 35-37] Similar results were obtained using $[Ir(COE)_2(\mu\text{-}TFA)]_2$ (TFA = trifluoroacetate) and $[Ir(C_2H_4)_2(\mu\text{-}Cl)]_2$ as the Ir source with [(5-FP)Ir(η^2,η^2-COD)][Ir(TFA)$_2$(η^2,η^2-COD)] (**1c**, Figure 3b) and [(5-FP)Ir(C_2H_4)$_2$][$IrCl_2$(C_2H_4)$_2$] (**1d**) as products (Scheme 4). The bond lengths in the cation [(5-FP)Ir(η^2,η^2-COD)]$^+$ of **1b** and **1c** are equal within standard deviation, and both species possess a mirror plane of symmetry (Table 1). Similarly, 5-^{Me}FP (**3**) reacts with

$[Ir(C_2H_4)_2(\mu\text{-}Cl)]_2$ to give $[(5\text{-}^{Me}FP)Ir(C_2H_4)_2][IrCl_2(C_2H_4)_2]$ (**3d**) (Scheme 4). The anion $[IrCl_2(C_2H_4)_2]^-$ appears as two broad peaks in the ^1H NMR spectrum, indicating a relatively high rotational barrier of the coordinated ethylene (Figure 4). The distances between the Ir center and the closest two carbons on the capping arene moiety reveal very weak to no η^2 interaction, similar to that of (5-^{X}FP)Rh complexes (Table 1).

Scheme 4. Syntheses of [(5-FP)Ir(COD)][$IrCl_2$(COD)] (**1b**), [(5-FP)Ir(COD)][$Ir(TFA)_2$(COD)] (**1c**), [(5-FP)Ir(C_2H_4)$_2$][$IrCl_2(C_2H_4)_2$] (**1d**) and [(5-^{Me}FP)Ir(C_2H_4)$_2$][$IrCl_2(C_2H_4)_2$] (**3d**).

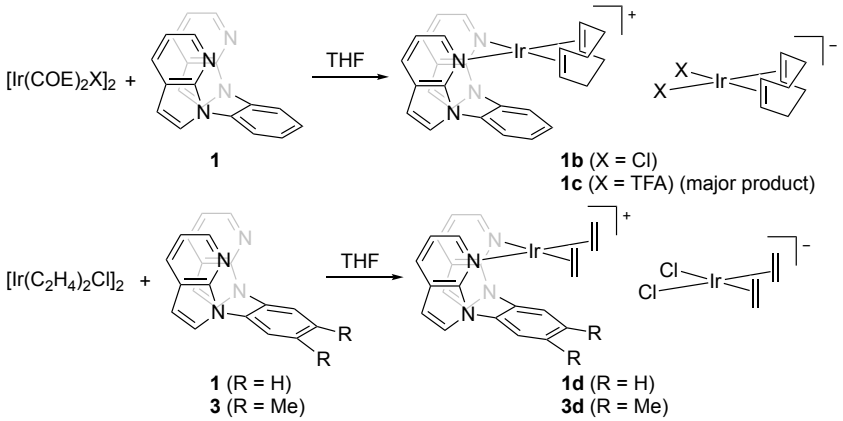

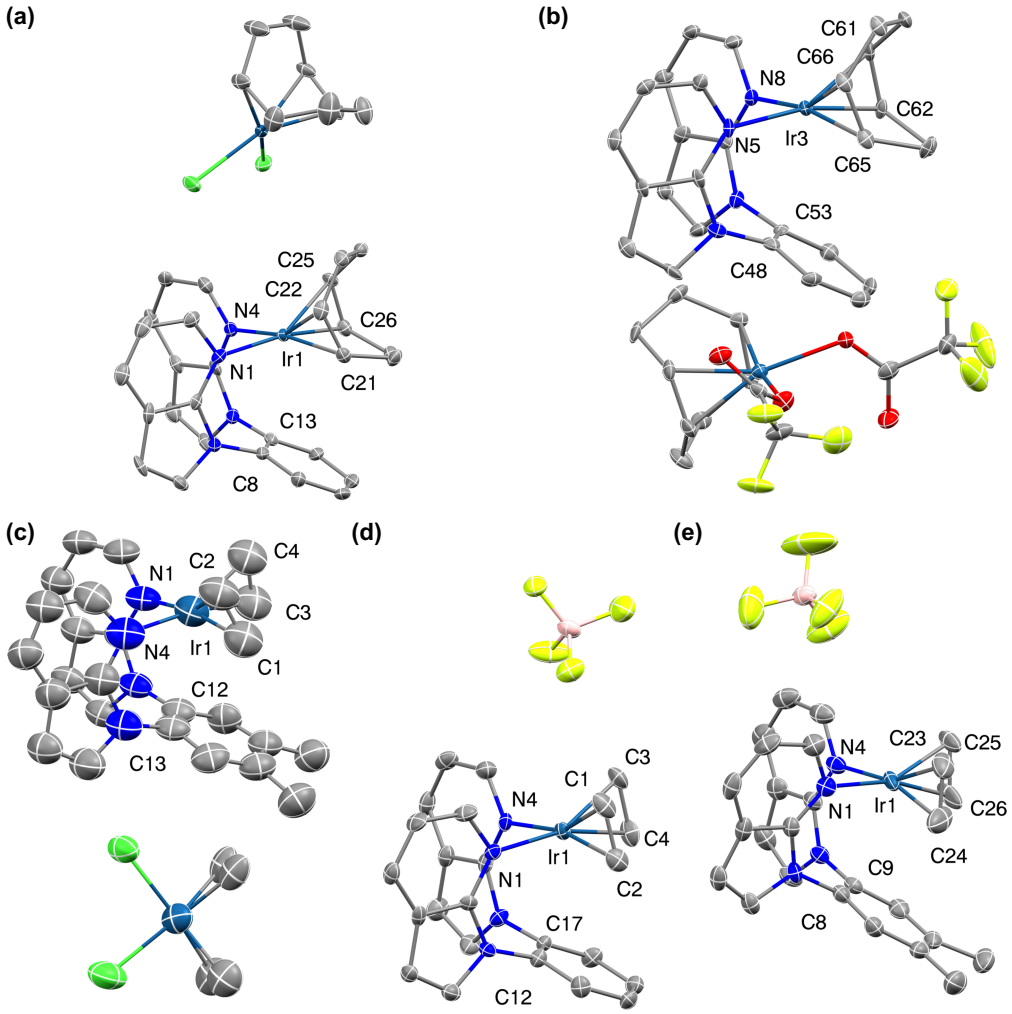

Figure 3. ORTEPs of [(5-FP)Ir(COD)][$IrCl_2$(COD)] (**1b**, a), [(5-FP)Ir(COD)][Ir(TFA)$_2$(COD)] (**1c**, b), [(5-^{Me}FP)Ir(C_2H_4)$_2$][$IrCl_2$(C_2H_4)$_2$] (**3d**, c), [(5-FP)Ir(C_2H_4)$_2$][BF_4] (**1e-BF_4**, d) and [(5-^{Me}FP)Ir(C_2H_4)$_2$][BF_4] (**3e-BF_4**, e). Ellipsoids are drawn at the 50% probability level, and hydrogen atoms are omitted for clarity.

Table 1. Selected bond lengths or distances between atoms for [(5-FP)Ir(COD)][$IrCl_2$(COD)] (**1b**), [(5-FP)Ir(COD)][Ir(TFA)$_2$(COD)] (**1c**), [(5-^{Me}FP)Ir(C_2H_4)$_2$][$IrCl_2$(C_2H_4)$_2$] (**3d**), [(5-FP)Ir(C_2H_4)$_2$][BF_4] (**1e-BF_4**) and [(5-^{Me}FP)Ir(C_2H_4)$_2$][BF_4] (**3e-BF_4**).

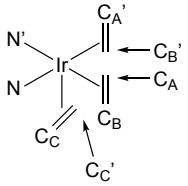

Bond	Bond length (Å)				
	1b	**1c**	**3d**	**1e-BF_4**	**3e-BF_4**
Ir–N	2.121(4)	2.103(8)	2.04(3)	2.106(5)	2.101(4)
Ir–N’	2.072(4)	2.101(8)	2.08(2)	2.111(5)	2.100(4)
Ir–C_A	2.120(4)	2.11(1)	2.14(3)	2.110(6)	2.121(5)
Ir–C_A’	2.127(4)	2.12(1)	2.10(4)	2.122(6)	2.141(5)

Ir–C_B	2.129(5)	2.13(1)	2.16(4)	2.110(7)	2.103(6)
Ir–C_B'	2.125(5)	2.111(9)	1.98(4)	2.111(5)	2.126(5)
Ir–C_C	3.192(5)	3.21(1)	3.11(3)	3.143(6)	3.144(4)
Ir–C_C'	3.149(5)	3.21(1)	3.07(3)	3.156(6)	3.132(4)
C_A–C_B	1.408(7)	1.43(2)	1.42(5)	1.378(9)	1.380(8)
C_A'–C_B'	1.412(7)	1.40(2)	1.30(4)	1.397(9)	1.403(7)

Note: C_C and C_C' are the two carbons of arene that are bound to the azaindolyl groups.

Silver(I) salts were added to the FP coordination reactions with Ir precursors in an attempt to abstract Cl from $[IrCl_2(C_2H_4)_2]^-$ to form $[(5\text{-FP})Ir(C_2H_4)_2]^+$. For example, mixing 5-FP, $[Ir(C_2H_4)_2Cl]_2$ and $AgBF_4$ in a 2:1:2 molar ratio in THF yields $[(5\text{-FP})Ir(C_2H_4)_2][BF_4]$ (**1e-BF$_4$**) (Scheme 5). The ^{1}H NMR spectrum of **1e-BF$_4$** reveals two resonances due to coordinated ethylene (3.22 and 1.63 ppm), which contrasts with $[(5\text{-FP})Ir(C_2H_4)_2][IrCl_2(C_2H_4)_2]$ (**1d**) as complex **1d** exhibits four resonances due to ethylene ligands (Figure 4). Based on the structure of $[(5\text{-FP})Ir(C_2H_4)_2]^+$ and the fact that ethylene rotation in $[IrCl_2(C_2H_4)_2]^-$ is slow on the NMR time scale, it is reasonable to expect four resonances (H_A, H_B, H_C and H_D) for C_2H_4 in the ^{1}H NMR spectrum of **1d**. A single crystal X-ray diffraction study confirmed the structure of **1e-BF$_4$** (Figure 3c). The key bond lengths of **1e-BF$_4$** are similar to those in **1b** and **1c** (Table 2). We were able to isolate the analogous Ir complex using 5-^{Me}FP, complex **3e-BF$_4$**, as shown in Scheme 5.

Scheme 5. Synthesis of $[(5\text{-FP})Ir(C_2H_4)_2][BF_4]$ (**1e-BF$_4$**) and $[(5\text{-}^{Me}FP)Ir(C_2H_4)_2][BF_4]$ (**3e-BF$_4$**).

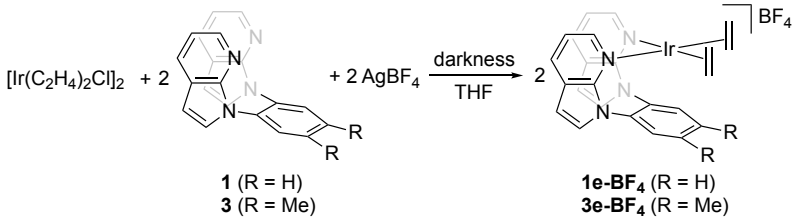

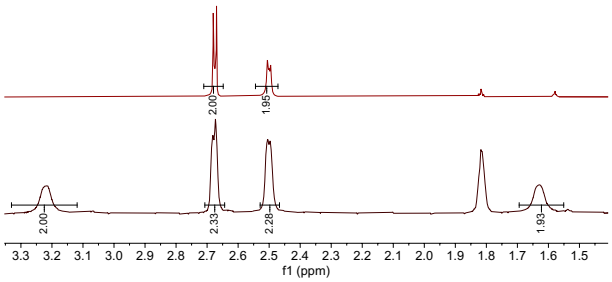

Figure 4. Coordinated ethylene region of ^{1}H NMR spectra of [(5-FP)Ir(C_2H_4)$_2$][IrCl_2(C_2H_4)$_2$] (**1d**) (bottom) and [(5-FP)Ir(C_2H_4)$_2$][BF_4] (**1e-BF_4**) (top). The resonances due to ethylene ligands are integrated.

In contrast to 5-FP (**1**) and 5-^{Me}FP (**3**), when using 5-^{NP}FP (**2**) as the ligand reactions with [Ir(COE)$_2$(μ-Cl)]$_2$ and [Ir(C_2H_4)$_2$Cl]$_2$ did not give the mixture of FP-Ir cation and [IrCl_2(C_2H_4)$_2$]$^-$. Mixing 5-^{NP}FP and [Ir(C_2H_4)$_2$(μ-Cl)]$_2$ in THF at room temperature results in two 5-^{NP}FP ligated Ir products in an approximate 20:1 ratio. The major product exhibits four triplets in the range of 4.2–2.8 ppm and 16 resonances in the aromatic region of the ^{1}H NMR spectrum, revealing an asymmetric complex, which is consistent with the structure of (5-^{NP}FP)Ir(C_2H_4)Cl (**2h**). The minor product, whose identity remains unknown, exhibits only eight peaks in the aromatic region of the ^{1}H NMR spectrum indicating the likely presence of σ-symmetry. In the case of the reaction between 5-^{NP}FP and [Ir(COE)$_2$(μ-Cl)]$_2$, one product is observed that is assigned as (5-^{NP}FP)Ir(COE)Cl (**2f**). Charging ethylene gas into a dichloromethane (DCM) solution of **2f** produces complex **2h** (Scheme 6).

Scheme 6. Synthesis of Ir complexes with the 5-^{NP}FP ligand.

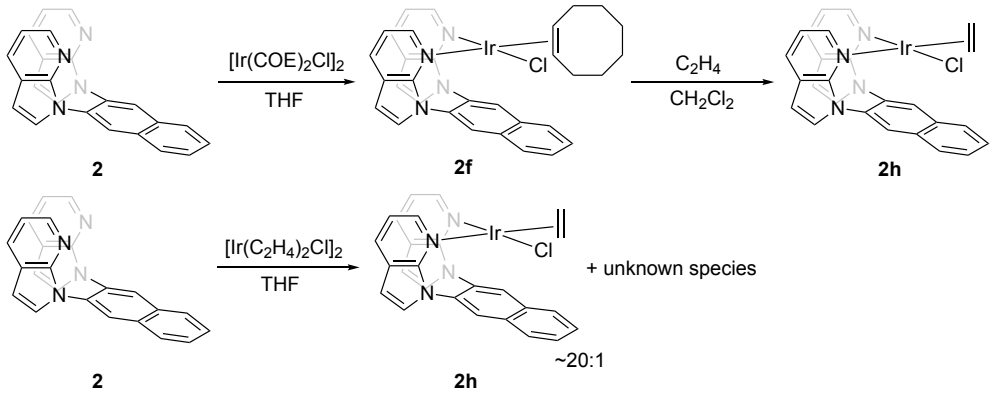

Synthesis and Characterization of (6-FP)Ir(C_2H_4)X. For the 6-^{X}FP ligand series, complexes of the type (6-^{X}FP)Ir(C_2H_4)X were observed as products upon reaction of 6-^{X}FP proligands with Ir dimers, which is different from the results for 5-FP (**1**) and 5-^{Me}FP (**3**) where bis-olefin coordinated complexes are formed. The complex (6-FP)Ir(C_2H_4)Cl (**4h**) was prepared by mixing 6-FP and [Ir(C_2H_4)$_2$(μ-Cl)]$_2$. The complex (6-FP)Ir(C_2H_4)(OAc) (**4i**) was synthesized using TlOAc to substitute Cl with OAc, and (6-FP)Ir(C_2H_4)(TFA) (**4j**) was made by charging ethylene gas into the reaction mixture of [Ir(COE)$_2$(μ-TFA)]$_2$ and 6-FP. In the synthesis of **4j**, prior to reaction with ethylene multiple products were observed with one of them identified as (6-FP)Ir(COE)(TFA) (**4g**) (Scheme 7).

Scheme 7. Synthesis of (6-FP)Ir(C_2H_4)Cl (**4h**), (6-FP)Ir(C_2H_4)(OAc) (**4i**) and (6-FP)Ir(C_2H_4)(TFA) (**4j**).

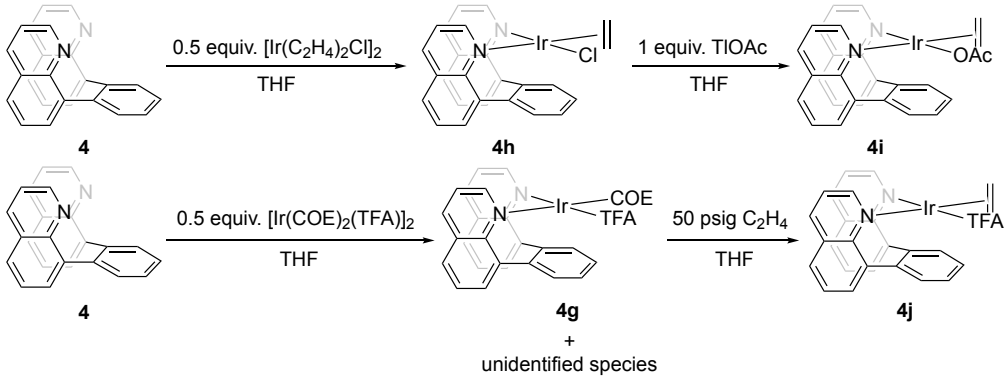

The ^{1}H NMR spectra of **4h**, **4i** and **4j** are similar to those of (6-FP)Rh(C_2H_4)X complexes. For each complex, a total of 16 resonances are observed, which is consistent with asymmetric structures. Similar to the 6-^{X}FP ligated Rh complexes and (5-^{NP}FP)Ir(C_2H_4)Cl (**2h**), for complexes **4h**-**4i** four resonances due to the coordinated ethylene are observed (^{1}H NMR spectroscopy), but a difference is that distinct triplet of doublets are observed for the ethylene resonances of **4h**, **4i** and **4j**, exhibiting $^{3}J_{HH}$ of ~9 Hz and $^{2}J_{HH}$ of ~1–2 Hz (Figure 5). Also, ethylene resonances of **4h**, **4i** and **4j** in ^{13}C{^{1}H} NMR spectra are observed as sharp peaks in the range of 15 to 35 ppm (Figure 5), while the resonances due to Rh complexes are all broad, which is likely due to the more rapid rate of rotation of ethylene for the Rh complexes as well as Rh-C coupling.[5,38]

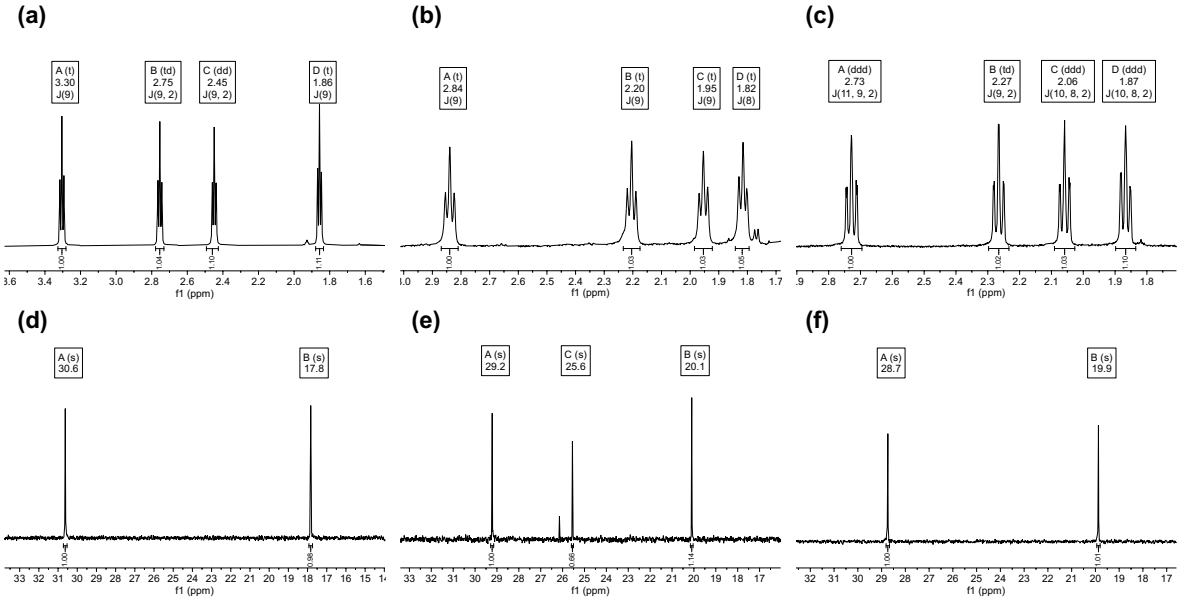

Figure 5. Coordinated ethylene region for (6-FP)Ir(C_2H_4)Cl (**4h**, a and d), (6-FP)Ir(C_2H_4)(OAc) (**4i**, b and e) and (6-FP)Ir(C_2H_4)(TFA) (**4j**, c and f) in ^{1}H NMR spectra (top) and ^{13}C{^{1}H} NMR spectra (bottom). The peak at 25.6 ppm in (e) is due to the methyl group on the acetate ligand.

X-ray structures from single crystals of **4h**, **4i** and **4j** exhibit obvious η^2 interactions between the Ir centers and the 1,2-carbons of the arene (Figure 6). The distances between Ir and the two carbon atoms

range from 2.2 Å to 2.5 Å (Table 2), which are much shorter than the same bond distances for 5-^{X}FP Ir complexes, which are in the range of 3.0 Å to 3.3 Å. The geometries at Ir of **4h**, **4i** and **4j** are closer to trigonal bipyramidal rather than square planar, which is similar to observations for (6-FP)Rh(C_2H_4)Cl (**4a**). The Cl or O atom and one of the N atoms are in the axial position (bond angles for corresponding N–Ir–X are: 174.72(7) °, 175.31(12) ° and 177.25(10) ° for **4h**, **4i** and **4j**, respectively), while the other N atom, ethylene ligand and the η^2-*C*,*C* interaction between the Ir and arene are in the equatorial positions.

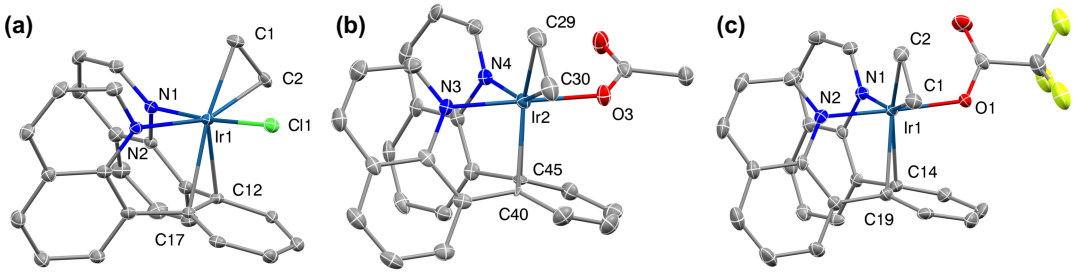

Figure 6. ORTEPs of (6-FP)Ir(C_2H_4)Cl (**4h**, a), (6-FP)Ir(C_2H_4)(OAc) (**4i**, b) and (6-FP)Ir(C_2H_4)(TFA) (**4j**, c). Ellipsoids are drawn at the 50% probability level, and hydrogen atoms are omitted for clarity.

Table 2. Selected bond lengths for (6-FP)Ir(C_2H_4)Cl (**4h**), (6-FP)Ir(C_2H_4)(OAc) (**4i**) and (6-FP)Ir(C_2H_4)(TFA) (**4j**).

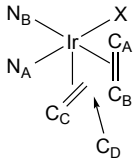

Bond	Bond lengths (Å)		
	4h	4i	4j
Ir–N_A	2.029(3)	2.030(3)	2.009(3)
Ir–N_B	2.195(3)	2.177(3)	2.175(3)
Ir–X	2.3643(8)	2.054(3)	2.070(2)
Ir–C_A	2.085(3)	2.078(5)	2.078(3)
Ir–C_B	2.079(3)	2.088(5)	2.072(3)
Ir–C_C	2.297(3)	2.244(4)	2.303(3)
Ir–C_D	2.353(3)	2.318(4)	2.410(3)
C_A–C_B	1.462(5)	1.469(7)	1.443(5)
C_C–C_D	1.440(4)	1.351(6)	1.427(5)

Note: C_C and C_D are the two carbons of arene that are bound to the quinoline groups.

Synthesis and Characterization of Ir Olefin Complexes Bearing 6-^{X}FP Ligands and "Abnormal" η^2-Arene Coordination. As discussed above, mixing 6-FP and $[Ir(COE)_2(\mu\text{-}TFA)]_2$ gives multiple products, with one product identified as (6-FP)Ir(COE)(TFA) (**4g**) (Figure 7a). Similar reactions were attempted for 6-^{NP}FP (**5**) and 6-^{F}FP (**7**), and neither of these proligands gave clean reactions with $[Ir(COE)_2(\mu\text{-}TFA)]_2$ (Scheme 8). Similar to the reaction that generates **4g**, (6-^{NP}FP)Ir(COE)(TFA) (**5g**) and (6-^{F}FP)Ir(COE)(TFA) (**7g**) were identified from the reaction mixtures by growing crystals and using X-ray diffraction studies (Figures 7b and 7d). The crystal structures of **4g** and **7g** are similar to that of (6-FP)Ir(C_2H_4)(TFA) (**4j**) but with longer Ir–C (η^2-olefin) bond distances (approximately 2.10 Å vs. approximately 2.07 Å, Tables 3 and 4). However, the crystal structure of (6-^{NP}FP)Ir(COE)(TFA) (**5g**) exhibits an η^2 coordination with the arene moiety at the 1,2-position of naphthalene rather than the "normal" 2,3-position (Figure 7d). The bonding interaction between Ir and the naphthalene group results in distortion of the Ir complex, better fitting a trigonal bipyramidal geometry. Here, we define the Ir/naphthalene interaction at the 1,2-position as "abnormal" η^2 coordination, since it is atypical from our studies of capping arene Rh(I), Rh(III), and Ir(I) complexes (Scheme 9).[1-3] The length of Ir–N bonds, which contain the N atom in the equatorial position of the approximately trigonal bipyramidal structure, is 2.271(3) Å, which is longer than typical Ir–N bond lengths.[39]

Mixing 6-^{NP}FP (**5**) and $[Ir(COE)_2(\mu\text{-}Cl)]_2$ in THF cleanly gives the product (6-^{NP}FP)Ir(COE)Cl (**5f**) (Scheme 8). The ^{1}H NMR spectrum of **5f** shows 18 resonances, which is consistent with the proposed asymmetric structure. The resonances of the two coordinated carbon atoms of the COE ligand are located at 60.6 and 46.8 ppm in the $^{13}C\{^1H\}$ NMR spectrum of **5f**. The two carbon atoms participating in the η^2 interaction with the Ir center resonate at 74.5 and 59.2 ppm, which can be easily distinguished

from other carbons in the ligand, which typically resonate between 160 and 110 ppm, due to the upfield chemical shifts. In the HSQC spectrum of **5f**, one of these two carbons is found to couple with a proton that appears as a singlet in the ^{1}H NMR spectrum and demonstrates no coupling to other protons in the COSY spectrum (Figure 8), indicating that the structure observed in the solid-state likely persists in solution. These observations are in agreement with the similar complex (6-^{NP}FP)Ir(COE)(TFA) (**5g**), where the η^2 interaction occurs at 1,2-position of naphthalene (Figure 7c). Similar to **5g**, **5f** also has an elongated Ir–N bond (Table 3). Charging ethylene gas into the solution of **7g**, **5f** or **5g** results in the formation of (6-^{F}FP)Ir(C_2H_4)(TFA) (**7j**), (6-^{NP}FP)Ir(C_2H_4)Cl (**5h**) and (6-^{NP}FP)Ir(C_2H_4)(TFA) (**5j**) as observed by *in situ* ^{1}H NMR spectroscopy.

Scheme 8. Reactions generating (6-FP)Ir(COE)(TFA) (**4g**), (6-^{NP}FP)Ir(COE)(TFA) (**5g**), (6-^{F}FP)Ir(COE)(TFA) (**7g**) and (6-^{NP}FP)Ir(COE)Cl (**5f**) as products.

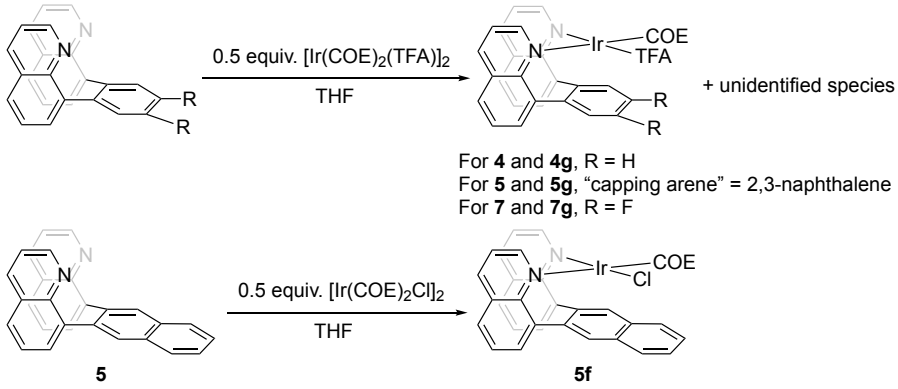

Scheme 9. The η^2 interaction (red dashed lines) between metal center and arene moiety in "normal" and "abnormal" coordination modes. The carbons interacting with metal are labelled with red arrows in the top view of the complexes. Other ligands on the metal center are omitted for clarity.[5]

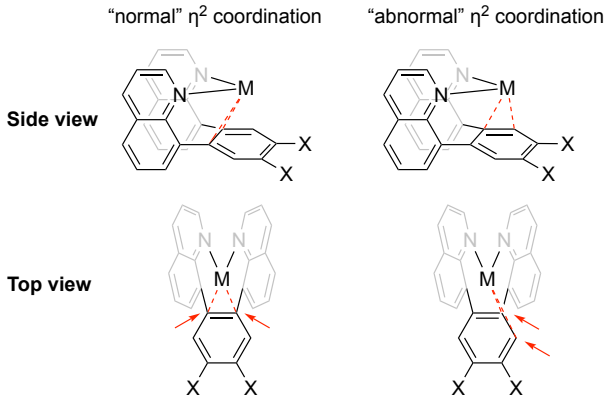

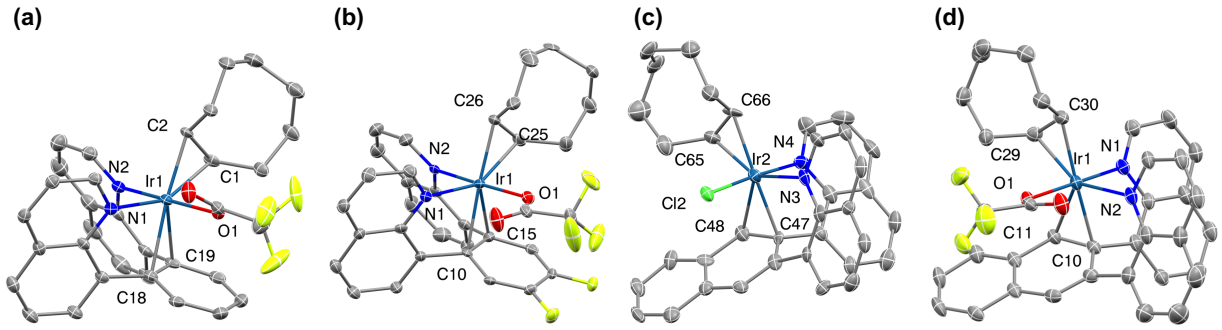

Figure 7. ORTEP drawings of (6-FP)Ir(COE)(TFA) (**4g**, a), (6-^{F}FP)Ir(COE)(TFA) (**7g**, b), (6-^{NP}FP)Ir(COE)Cl (**5f**, c) and (6-^{NP}FP)Ir(COE)(TFA) (**5g**, d). Ellipsoids are drawn at the 50% probability level, and hydrogen atoms are omitted for clarity.

Table 3. Selected bond lengths for (6-FP)Ir(COE)(TFA) (**4g**), (6-^{F}FP)Ir(COE)(TFA) (**7g**), (6-^{NP}FP)Ir(COE)Cl (**5f**) and (6-^{NP}FP)Ir(COE)(TFA) (**5g**).

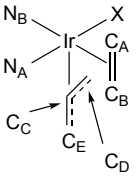

Bond	Bond length (Å)			
	4g	**7g**	**5f**	**5g**
Ir–N_A	2.018(3)	2.025(4)	2.068(7)	2.038(3)
Ir–N_B	2.188(3)	2.183(4)	2.269(6)	2.271(3)
Ir–X	2.056(3)	2.053(4)	2.361(2)	2.068(2)
Ir–C_A	2.101(4)	2.107(5)	2.130(9)	2.100(4)
Ir–C_B	2.101(4)	2.104(5)	2.077(9)	2.096(4)
Ir–C_C	2.300(4)	2.247(5)	2.140(8)	2.161(4)
Ir–C_D	2.323(4)	2.266(5)	N/A	N/A

Ir–C_E	N/A	N/A	2.207(8)	2.236(3)

Note: C_C and C_D are the two carbons on the "capping arene" bonding with the quinoline moiety.

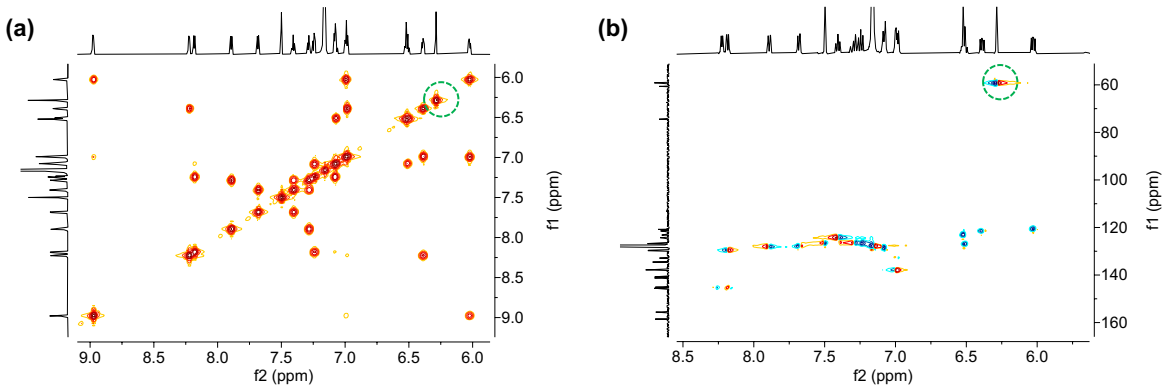

Figure 8. The 6-^{NP}FP region of COSY (left) and HSQC (right) spectra of (6-^{NP}FP)Ir(COE)Cl (**5f**). The resonance of the carbon in the η^2 coordination and its bonding proton signals are circled.

The complexes (6-^{NP}FP)Ir(C_2H_4)Cl (**5h**), (6-^{Me}FP)Ir(C_2H_4)Cl (**6h**) and (6-^{F}FP)Ir(C_2H_4)Cl (**7h**) were synthesized using the same method as (6-FP)Ir(C_2H_4)Cl (**4h**) (Scheme 10). The abnormal η^2 coordination was also observed for these complexes, as indicated by the HSQC spectra (Figures S44, S48 and S53) and confirmed by the X-ray crystal structures of **6h** and **7h** (Figure 9). There are two peaks in the ^{19}F NMR spectrum of **7h**, both appearing with a ddd splitting pattern, which is consistent with an asymmetric structure. Compared with the normal η^2 coordination in (6-FP)Ir(C_2H_4)Cl (**4h**), the abnormal η^2 coordination seems to be stronger based on the distances of Ir to the two carbons, which might be a driving force of the distortion. In (6-FP)Ir(C_2H_4)Cl (**4h**), the distances between Ir and the two coordinating carbons are 2.297(3) and 2.353(3) Å, which are slightly longer than (6-^{Me}FP)Ir(C_2H_4)Cl (**6h**) (2.197(4) and 2.308(4) Å) and (6-^{F}FP)Ir(C_2H_4)Cl (**7h**) (2.173(9) and 2.238(9) Å) (Table 3 and Table 4).[40-42]

Scheme 10. Synthesis of (6-^{NP}FP)Ir(C_2H_4)Cl (**5h**), (6-^{Me}FP)Ir(C_2H_4)Cl (**6h**) and (6-^{F}FP)Ir(C_2H_4)Cl (**7h**).

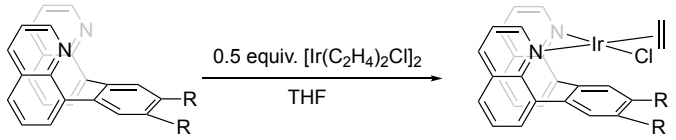

For **5** and **5g**, "capping arene" = 2,3-naphthalene
For **6** and **6g**, R = Me
For **7** and **7g**, R = F

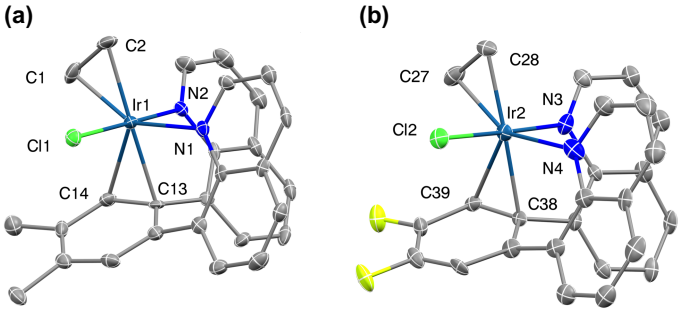

Figure 9. ORTEP drawings of (6-^{Me}FP)Ir(C_2H_4)Cl (**6h**, a) and (6-^{F}FP)Ir(C_2H_4)Cl (**7h**, b). Ellipsoids are drawn at the 50% probability level, and hydrogen atoms are omitted for clarity.

Table 4. Selected bond lengths for (6-^{Me}FP)Ir(C_2H_4)Cl (**6h**) and (6-^{F}FP)Ir(C_2H_4)Cl (**7h**).

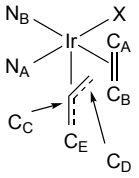

Bond	Bond length (Å)	
	6h	**7h**
Ir–N_A	2.052(4)	2.052(7)
Ir–N_B	2.266(4)	2.298(9)
Ir–X	2.3594(12)	2.373(2)
Ir–C_A	2.097(5)	2.087(9)
Ir–C_B	2.076(5)	2.068(10)
Ir–C_C	2.197(4)	2.173(9)
Ir–C_E	2.308(4)	2.238(9)
C_A–C_B	1.502(7)	1.458(14)

Note: C_C and C_D are the two carbons on the "capping arene" bonding with the quinoline moiety.

Rotation Barriers of Ethylene in (FP)M(C_2H_4)X and [(5-^{X}FP)Ir(C_2H_4)$_2$]BF_4 complexes. The rate of some fluxional processes can be measured when the rate is comparable with the NMR timescale.[43-

[45] For example, variable temperature NMR spectroscopy has been a useful tool to study the activation barrier for ethylene rotation of metal–ethylene complexes when the four hydrogen atoms are not symmetry equivalent in the thermodynamically preferred coordination mode.[46, 47] In such complexes, at a slower rate of ethylene rotation the coordinated ethylene resonates as four peaks in the ^{1}H NMR spectrum with clear splitting patterns (Scheme 11, H_A, H_B, H_C and H_D), as in the cases of most Ir–ethylene complexes in this work. When the rate of ethylene rotation is greater, the peaks due to ethylene broaden {e.g., the case of (6-^{NP}FP)Rh(C_2H_4)Cl (**5a**)} and can coalesce into two resonances at more rapid rates of ethylene rotation {Scheme 11, $H_A = H_C$, $H_B = H_D$; e.g., the case of (5-FP)Rh(C_2H_4)Cl (**1a**)}.

Scheme 11. Rotation of coordinated ethylene in M(η^2-C_2H_4) complex. In a static structure, the four hydrogen atoms are non-equivalent in an asymmetric complex.

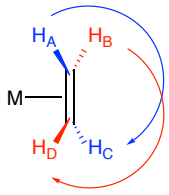

We found no obvious change in the NMR spectra when heating [(5-^{X}FP)Ir(C_2H_4)$_2$]BF_4 {5-^{X}FP = 5-FP (**1e-BF$_4$**) and 5-^{Me}FP (**3e-BF$_4$**)} complexes up to 145 °C, indicating the likelihood of substantial ethylene rotational barriers. Using the chemical shift difference between ethylene resonances for **1e-BF$_4$**, which is ~540 Hz, and the lack of observation of coalescence up to 145 °C, we can place a limit on the $\Delta G^{\ddagger}$ for ethylene rotation of $\geqslant$ 19 kcal/mol.

The ethylene peaks of (5-^{X}FP)Rh(C_2H_4)Cl complexes appear as two broad peaks in the ^{1}H NMR spectra, indicating that the peaks are coalesced at room temperature. The broad resonances could be a result of not yet reaching the fast exchange regime at room temperature, or they could be due to $^2J_{Rh-}$

$_H$ coupling. In contrast, (6-^{X}FP)Rh(C_2H_4)Cl complexes all display four resonances due to coordinated ethylene in room temperature ^{1}H NMR spectra with (6-FP)Rh(C_2H_4)Cl (**4a**) and (6-^{Me}FP)Rh(C_2H_4)Cl (**6a**) displaying four broad peaks and (6-^{NP}FP)Rh(C_2H_4)Cl (**5a**) showing four well-resolved doublets of doublets. The rotational barriers of ethylene for (5-^{X}FP)Rh(C_2H_4)X complexes were determined using variable temperature experiments in CD_2Cl_2 (Table 5 and Supporting Information). Different substituents on the capping arene did not result in a substantial difference in the activation barrier of ethylene rotation.

The rotational barriers of (6-^{X}FP)M(C_2H_4)X complexes were determined using variable temperature experiments in DMF-d_7 (Table 5, see Supporting Information). The coalescence temperatures (T_c) for Ir complexes (> 140 °C) are significantly larger than those for Rh complexes at 55 °C to 120 °C. For the Rh complexes **1a**-**4a** and **6a** (note: ethylene rotational barrier for **5a** could not be determined), the 5-FP complexes **1a**-**3a** show $\Delta G^{\ddagger}$'s (at T_c) between 10.4 and 14.1 kcal/mol. In contrast, the 6-FP Rh complexes **4a** and **6a** exhibit greater $\Delta G^{\ddagger}$'s (at T_c) of 21.1 and 20.4 kcal/mol, respectively. The Eyring analyses show that the $\Delta H^{\ddagger}$'s for **1a**-**3a**, ranging between 10.4 and 14.7 kcal/mol, are less than **4a** and **6a** at 22.2 and 21.6 kcal/mol, respectively. This is consistent with our hypothesis that the distance between the capping arene moiety and Rh plays an important role in other metal-ligand interactions. It is important to note that activation barriers for olefin rotation can depend on multiple factors,[44] and this is especially true of five-coordinate d^8 complexes for which impactful factors include geometry (trigonal bipyramidal versus square pyramidal), olefin coordination position (e.g., equatorial or axial), and π-acidity of ancillary ligands.[48-55] We provide one direct comparison between Rh and Ir complexes, **2a** and **2h**. The $\Delta G^{\ddagger}$ (at T_c) and the $\Delta H^{\ddagger}$ for Ir complex **2h** (15.3 kcal/mol 15.1 kcal/mol, respectively) are slightly larger than the Rh complex **2a** at 14.1 kcal/mol ($\Delta G^{\ddagger}$) and 13.9 kcal/mol ($\Delta H^{\ddagger}$).

Table 5. Coalescence temperatures and barriers for ethylene rotation of some (FP)M(C_2H_4)X complexes.

Complex	Solvent	T_c (°C)[a]	$\Delta H^‡$ (kcal·mol^{-1})	$\Delta S^‡$ (cal·mol^{-1}·K^{-1})	$\Delta G^‡$ at T_c (kcal·mol^{-1})
(5-FP)Rh(C_2H_4)Cl (**1a**)	DCM-d_2	−20	14.7(1.5)	12(6)	11.6(2.2)
(5-^{NP}FP)Rh(C_2H_4)Cl (**2a**)	DCM-d_2	−20	13.9(1.4)	10(5)	14.1(1.9)
(5-^{Me}FP)Rh(C_2H_4)Cl (**3a**)	DCM-d_2	0	10.4(3.6)	-6(13)	10.4(5.0)
(6-FP)Rh(C_2H_4)Cl (**4a**)	DMF-d_7	55	22.2(4.6)	24(14)	21.1(6.5)
(6-^{NP}FP)Rh(C_2H_4)Cl (**5a**)	DMF-d_7	N/A[b]	-	-	-
(6-^{Me}FP)Rh(C_2H_4)Cl (**6a**)	DMF-d_7	55	21.6(1.4)	19(5)	20.4(2.1)
(5-^{NP}FP)Ir(C_2H_4)Cl (**2h**)	DMF-d_7	75	15.1(0.4)	-3(1)	15.3(0.5)
(6-^{NP}FP)Ir(C_2H_4)Cl (**5h**)	DMF-d_7	> 145[c,d]	-	-	-

Notes: Standard errors are given in parenthesis and determined from a minimum of three data points. [a] T_c = coalescence temperature. [b] Reaction occurs at room temperature. [c] The upper limit of NMR instrument is 145 °C. [d] The initial broadening starts at 145 °C; thus, we were not able to obtain data for ethylene rotation.

DFT Calculations. To evaluate the extent of metal-to-olefin π-backbonding as a function of capping arene ligand, Density Functional Theory (DFT) calculations (at the M062X-D3 level, including van der Waals corrections) were utilized. To begin, we optimized the structures of the Rh complexes **1a**-**6a**. Upon coordination to d^n (n > 0) metal centers, ethylene C=C bond distances are often correlated with the magnitude of metal-to-olefin π-backbonding. A long C=C bond distance indicates more significant metal-to-olefin π-backbonding, and a shorter C=C bond distance indicates relatively reduced π-backbonding. Complexes **1a**-**3a** were calculated to have C=C bond distances of 1.39 Å (Table 6), which is approximately 0.05 Å longer than the C=C bond distance of 1.34 Å for free ethylene. The calculated C=C bond distance for the Rh complexes **4a**, **5a**, and **6a** are 1.40, 1.42, and 1.40 Å, respectively. Based solely on the elongation of the ethylene C=C bond lengths, we expect Rh-ethylene π-backbonding follows the trend **5a > 6a ~ 4a > 1a-3a**. These calculated C=C bond lengths are consistent with experimentally observed ethylene rotational barriers (Table 5).

Natural Bond Orbital (NBO) analysis was performed to provide a quantitative assessment of π-backbonding. Lee and coworkers previously utilized NBO analysis to correlate metal-olefin π-backbonding with antibonding π^* electron population on the olefin.[56] One feature of NBO analysis is that it calculates second-order perturbative charge transfer ΔE^2_{CT}. This value effectively allows estimation of donor-acceptor (bond-anti-bond) interaction in a system according to equation 1, where q_i is the donor occupancy (usually 2), F^2_{ij} is the off-diagonal element of the NBO Fock matrix,[57] and e_j and e_i are the acceptor and donor orbital energies, respectively.

$$\Delta E^2_{CT} = q_i \frac{F^2_{ij}}{e_j - e_i} \qquad (1)$$

ΔE^2_{CT} is considered a stabilization energy due to electron delocalization (departure from the ideal Lewis structure). We report values of ΔE^2_{CT} for complexes **1a**-**6a** (Table 6); here the donating orbital is an occupied d orbital on Rh while the accepting orbitals are the unoccupied π^* orbitals on ethylene. For complexes **1a**, **2a**, and **3a** we calculate ΔE^2_{CT} values of 0.21, 0.20, and 0.20 kcal·mol^{-1}, respectively. NBO analysis predicts ΔE^2_{CT} of 0.30 kcal·mol^{-1} for **4a** and 1.20 kcal·mol^{-1} for **5a**. Finally, **6a** is predicted to have a ΔE^2_{CT} of 0.29 kcal·mol^{-1}. We see that calculated ΔE^2_{CT} correlates with the calculated ethylene C=C distances. For the Rh complexes, there appears to be a correlation between ΔE^2_{CT} and the experimentally observed barriers for ethylene rotation reported in Table 5 (Figure 10a). However, the Ir complex **2h** appears to be an outlier.

Table 6. Important distances in Å and ΔE^2_{CT} in kcal·mol^{-1} for select complexes calculated by DFT.

Complex	[M] - C_{cap} (Å)	C=C (Å)	ΔE^2_{CT} (kcal·mol^{-1})
(5-FP)Rh(C_2H_4)Cl (**1a**)	3.16	1.39	0.21
(5-^{NP}FP)Rh(C_2H_4)Cl (**2a**)	3.16	1.39	0.20
(5-^{Me}FP)Rh(C_2H_4)Cl (**3a**)	3.15	1.39	0.20
(6-FP)Rh(C_2H_4)Cl (**4a**)	2.97	1.40	0.30
(6-^{NP}FP)Rh(C_2H_4)Cl (**5a**)	2.68	1.42	1.20

(6-^{Me}FP)Rh(C_2H_4)Cl (**6a**)	2.95	1.40	0.29
(5-^{NP}FP)Ir(C_2H_4)Cl (**2h**)	3.15	1.42	0.46
(6-FP)Ir(C_2H_4)Cl (**4h**)	2.80	1.44	1.22
(6-^{NP}FP)Ir(C_2H_4)Cl (**5h**)	2.21	1.45	3.59
(6-^{Me}FP)Ir(C_2H_4)Cl (**6h**)	2.41	1.45	4.41
(6-^{F}FP)Ir(C_2H_4)Cl (**7h**)	2.28	1.45	4.29

Note: [M] - C_{cap} is the average distance between the metal center and the adjacent C's of the capping arene.

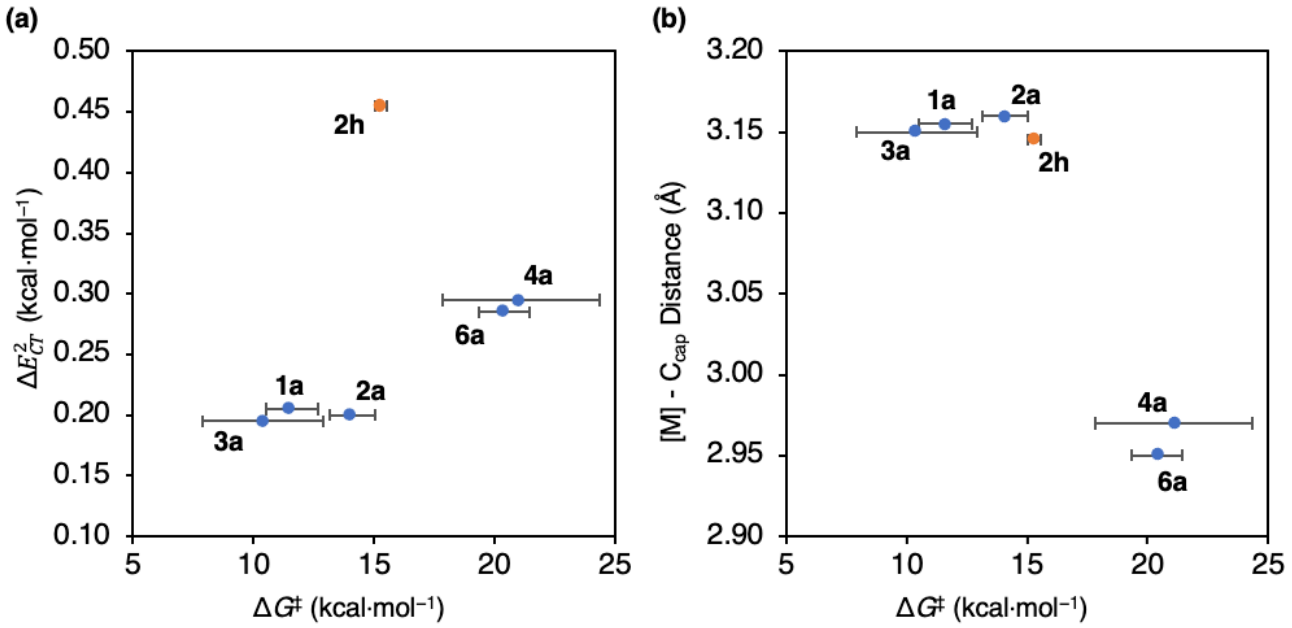

Figure 10. (a) Experimentally observed barrier for ethylene rotation ($\Delta G^{\ddagger}$, in kcal·mol^{-1}) vs. charge transfer stabilization (ΔE_{CT}^2, in kcal·mol^{-1}) for available complexes. **(b)** Experimentally observed barrier for ethylene rotation vs. the average calculated bond distance between the metal center and the two adjacent C's of the capping arene ([M] – C_{cap}, in Å). Data points are labeled by complex identity. Standard errors of the experimental ethylene rotation barriers are depicted by error bars.

The Rh complexes show a correlation between the experimentally observed barrier for ethylene rotation and the DFT-calculated charge transfer stabilization. However, some of the calculated ΔE_{CT}^2 values are within > 0.1 kcal·mol^{-1} of each other, which is within the error of DFT. For the FP-ligated complexes, a more apt predictor for metal-olefin π-backbonding may instead be the calculated average distance between the metal center and the two adjacent C's of the capping arene ligand. Plotting the

calculated bond distances between Rh and the two bonded carbon atoms of the capping arene ligand versus experimental activation barrier for ethylene rotation reveals two clusters: one for the 5-FP complexes and one for the 6-FP complexes (Figure 10b). Using the available data, we find a relation between the experimental ethylene rotation barrier and the [M]–C_{cap} distance.

Also, we optimized the structures of the Ir complexes **2h** and **4h** - **7h.** The calculated ethylene C=C bond distance is 1.42 Å for **2h** and 1.44 Å for **4h**. For complexes **5h**-**7h** the C=C bond distances are all calculated to be 1.45 Å. These calculated bond distances indicate that Ir-ethylene π-backbonding follows the trend **5h**-**7h** > **4h** > **2h**. The calculated ΔE_{CT}^2s for the backbonding interactions between Ir and ethylene are summarized in Table 6. The π-backbonding charge transfer energy is lowest for **2h** and **4h**, suggesting these complexes have the least Ir-ethylene π-backbonding character. The calculated charge transfer is significantly higher for complexes **5h**-**7h**, signifying strong electron donation from the Ir d orbital to the ethylene π^* space. These calculated data are consistent with calculations and experimental data for the Rh complexes.

■ SUMMARY AND CONCLUSIONS

A series of Rh^I/Ir^I η^2-olefin complexes bearing "capping arene" ligands were synthesized and characterized. Seven "capping arene" ligands offer various metal–arene distances as well as other steric properties to potentially influence olefin coordination. Consistent with our hypothesis, observed geometries of complexes with 5-^{X}FP ligands indicate that these ligands will provide complexes with 16-electron square planar structures while 6-^{X}FP ligands are more likely to donate two additional electrons through the arene group, forming 18-electron complexes. Thus, 6-^{X}FP ligands more likely serve as a

tridentate ligand through a combination of κ^2 and η^2 binding modes and provide a trigonal bipyramidal geometry. Combined experimental and computational studies suggest that the greater donor ability of 6-FP ligands, compared with 5-FP ligands, results in more substantial ethylene rotational barriers. We proposed that these differences are likely a result of the ligand structures, which dictate metal-arene distances and, hence, the extent of arene to metal electron donation (Scheme 12).

Scheme 12. Impact of structure of capping arene ligand on metal electron density, metal-to-olefin π-backbonding, and ethylene rotational barrier (M = Rh or Ir).

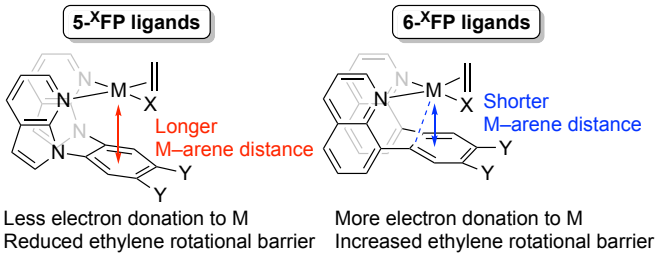

EXPERIMENTAL SECTION

General Methods. Unless otherwise noted, all reactions and manipulations were performed under a dinitrogen atmosphere in a glovebox or using standard Schlenk techniques with dried and degassed solvents. All solvents were reagent grade or better and were purified by distillation and/or passage through a column of alumina and kept in the glovebox over 4Å molecular sieves. All NMR spectra were recorded on a Varian Inova 600 MHz or 500 MHz spectrometer, or a Bruker Avance III 800 MHz spectrometer. The operating frequency for $^{13}C\{^1H\}$ NMR is 150 MHz (on 600 MHz instrument) or 201 MHz (on 800 MHz instrument), and for ^{19}F NMR the operating frequency is 564 MHz (on 600 MHz instrument). All ^1H and $^{13}C\{^1H\}$ NMR spectra were referenced against respective residual ^1H or $^{13}C\{^1H\}$ resonances of the deuterated solvents. All spectra were recorded at room temperature (~25 °C) unless

otherwise indicated. Methanol-d_4 and ethylene glycol were used to calibrate the temperature in variable temperature NMR experiments.[58] Literature procedures were used to prepare $[Rh(C_2H_4)_2(\mu\text{-}Cl)]_2$, $[Ir(C_2H_4)_2(\mu\text{-}Cl)]_2$, $[Ir(COE)_2(\mu\text{-}Cl)]_2$, $[Ir(COE)_2(\mu\text{-}TFA)]_2$, 5-FP (**1**), 5-^{NP}FP (**2**), 6-^{NP}FP (**5**), 6-^{Me}FP (**6**), 6-^{F}FP (**7**), (5-FP)$Rh(C_2H_4)Cl$ (**1a**), (5-^{NP}FP)$Rh(C_2H_4)Cl$ (**2a**), (6-FP)$Rh(C_2H_4)Cl$ (**4a**), and (6-^{NP}FP)$Rh(C_2H_4)Cl$ (**5a**).[1-3, 33, 35, 59-61] Other reagents were from commercial sources and used as received. All the assignments for NMR spectra are given and relative to the numbers in the structure below.

Synthesis and characterization. 5-^{Me}FP (3). The procedure was modified from a published procedure.[33] In a 100 mL pressure flask, 7-azaindole (7.09 g, 60 mmol), 4,5-dibromoxylene (6.60 g, 25 mmol), CuI (0.95 g, 5 mmol), 1,10-phenanthroline (1.80 g, 10 mmol), Cs_2CO_3 (34.2 g, 105 mmol), and dodecane (2.25 mL) were mixed in DMF (15 mL). The reaction mixture was heated at 150 °C for 3 days. After the reaction mixture cooled to room temperature, it was filtered through a fine porosity frit loaded with Celite, which was washed with 10 mL of DMF. Next, 100 mL of water were added to the filtrate, yielding a brown suspension. A total of 600 mL of Et_2O were added in three subsequent additions to extract the product, and the Et_2O solution was dried over Na_2SO_4. The solvent was removed under reduced pressure, yielding a brown oil. Column chromatography was performed using basic alumina as the stationary phase. A hexanes/ethyl acetate mix (5:1 v/v, then 3:1) was used as the eluent. The solvent was removed from the eluent, and the product was recrystallized using hexanes and methylene chloride. The product was obtained as a white solid with an isolated yield of 82% (6.9 mg). See below for structure and assignments. ^{1}H NMR (600 MHz, CD_2Cl_2): δ 8.16 (dd, $^3J_{HH}$ = 5 Hz, $^4J_{HH}$ = 2 Hz, 2H, *3* position), 7.80 (dd, $^3J_{HH}$ = 8 Hz, $^4J_{HH}$ = 2 Hz, 2H, *1* position), 7.49 (s, 2H, *6* position), 7.02 (dd, $^3J_{HH}$ = 8 Hz, $^3J_{HH}$ = 5 Hz, 2H, *2* position), 6.82 (d, $^3J_{HH}$ = 4 Hz, 2H, *4* or *5* position), 6.24 (d, $^3J_{HH}$ = 4 Hz, 2H, *4* or *5* position), 2.43

(s, 6H, C*H*$_3$). $^{13}C\{^1H\}$ NMR (151 MHz, CD_2Cl_2): δ 149.0 (s), 143.9 (s), 138.2 (s), 132.6 (s), 130.5 (s), 129.3 (s), 129.0 (s), 120.8 (s), 116.8 (s), 101.2 (s), 19.9 (s). HRMS (ESI) (m/z) $[M+H]^+$ calcd for $C_{22}H_{18}N_4$: 339.1604. Found: 339.1608.

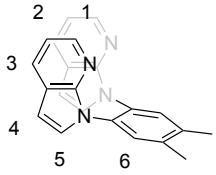

6-FP (4). The procedure was modified from a published synthesis.[5] Quinolin-8-ylboronic acid (3.00 g, 17.3 mmol, 2.4 equiv.), 1,2-diiodobenzene (2.39 g, 7.24 mmol, 1 equiv.), Cs_2CO_3 (23.9 g, 72.4 mmol, 10 equiv.), $Pd(PPh_3)_4$ (0.81 g, 0.72 mmol, 0.1 equiv.) and DMF (120 mL) were combined into a 250 mL pressure flask in the glovebox. The reaction mixture was sealed and stirred in an oil bath at 115 °C for 24 h. After cooling to room temperature, the reaction mixture was filtered through a fine porosity frit and loaded with Celite. Next, 250 mL of DI water was added to the DMF solution, resulting in a yellowish suspension. Methylene chloride (200 mL) was added to extract the product from the DMF-water layer (repeated twice). The resulting methylene chloride solution was dried using sodium sulfate, filtered, and the solvent was removed from the filtrate under reduced pressure, resulting in a brown oil. The product was purified by column chromatography using silica gel. A mixture of hexanes and ethyl acetate (5:1 v/v, then 3:1) with a few drops of triethylamine was used as the eluent. The product fraction was collected and activated charcoal was added, turning the yellow solution colorless (this step can be skipped if the fraction is already colorless). The solvent was removed under vacuum, affording a colorless oil. The product precipitated out of solution when 200 mL of *n*-pentane was added and was collected as white powder after removing the *n*-pentane under vacuum. Purity and identity were determined by comparison to previously reported NMR data.[5] The isolated yield was 65% (1.56 g). X-ray quality crystals of 6-FP

were obtained by vapor diffusion using THF and *n*-pentane. See below for structure and assignments. ^{1}H NMR (800 MHz, C_6D_6): δ 8.72 (br, 2H, *1* position), 7.77 (dd, AA'BB', $^{3}J_{HH}$ = 7, 5 Hz, 2H, *7* or *8* position), 7.53 (d, $^{3}J_{HH}$ = 7 Hz, 2H, *4* or *6* position), 7.41 (br, 2H, *3* position), 7.38 (dd, AA'BB', $^{3}J_{HH}$ = 7, 5 Hz, *7* or *8* position), 7.08 (dd, $^{3}J_{HH}$ = 8 Hz, $^{4}J_{HH}$ = 1 Hz, 2H, *4* or *6* position), 6.75 (br, 2H, *5* position), 6.71 (br, 2H, *2* position). ^{13}C{^{1}H} NMR (201 MHz, C_6D_6): δ 149.8 (br), 147.6 (br), 142.4 (s), 140.3 (s), 135.5 (br), 132.4 (s), 131.3 (s), 128.4 (s), 126.9 (s), 126.7 (s), 125.7 (s), 120.7 (s).

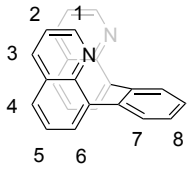

(5-^{Me}FP)Rh(C_2H_4)Cl (3a). In a round bottom flask, a THF solution (20 mL) of 5-^{Me}FP (175 mg, 514 μmol) was added to a THF solution (30 mL) of $[Rh(C_2H_4)_2Cl]_2$ (100 mg, 257 μmol). The reaction mixture was allowed to stir overnight, during which time the solution turned from orange to brown. The solvent was removed under vacuum to give a dark brown solid. The crude solid was dissolved in a minimal amount of methylene chloride, and 50 mL of *n*-pentane was added to precipitate a yellow solid, which was then dried under vacuum. The isolated yield was 82% (212 mg). See below for structure and assignments. ^{1}H NMR (800 MHz, CD_2Cl_2, 25 °C): δ 8.96 (d, $^{3}J_{HH}$ = 5 Hz, 1H, *1* or *1*' position), 8.44 (d, $^{3}J_{HH}$ = 6 Hz, 1H, *1* or *1*' position), 7.76 (d, $^{3}J_{HH}$ = 8 Hz, 1H, *3* or *3*' position), 7.58 (m, 2H, *6* or *6*', *3* or *3*' position), 7.25 (d, $^{3}J_{HH}$ = 4 Hz, 1H, *4*, *4*', *5* or *5*' position), 7.24 (s, 1H, *6* or *6*' position), 7.22 (d, $^{3}J_{HH}$ = 4 Hz, 1H, *4*, *4*', *5* or *5*' position), 7.04 (dd, $^{3}J_{HH}$ = 8, 5 Hz, 1H, *2* or *2*' position), 6.73 (dd, $^{3}J_{HH}$ = 8, 6 Hz, 1H, *2* or *2*' position), 6.45 (d, $^{3}J_{HH}$ = 4 Hz, 1H, *4*, *4*', *5* or *5*' position), 6.42 (d, $^{3}J_{HH}$ = 4 Hz, 1H, *4*, *4*', *5* or *5*' position), 2.52 (s, 3H, CH_3), 2.46 (s, 3H, CH_3), 2.91–2.32 (br, 4H, C_2H_4). ^{1}H NMR (497 MHz, CD_2Cl_2, −60 °C): δ 8.90 (d, $^{3}J_{HH}$ = 5 Hz, 1H, *1* or *1*' position), 8.45 (d, $^{3}J_{HH}$ = 6 Hz, 1H, *1* or *1*' position), 7.76 (d,

$^3J_{HH}$ = 8 Hz, 1H, *3* or *3*' position), 7.59 (d, $^3J_{HH}$ = 8 Hz, 1H, *3* or *3*' position), 7.53 (s, 1H, *6* or *6*' position), 7.27–7.24 (m, 2H, *4*, *4*', *5* or *5*' position), 7.22 (s, 1H, *6* or *6*' position), 7.03 (dd, $^3J_{HH}$ = 8, 5 Hz, 1H, *2* or *2*' position), 6.74 (dd, $^3J_{HH}$ = 8, 6 Hz, 1H, *2* or *2*' position), 6.45 (d, $^3J_{HH}$ = 4 Hz, 1H, *4*, *4*', *5* or *5*' position), 6.41 (d, $^3J_{HH}$ = 4 Hz, 1H, *4*, *4*', *5* or *5*' position), 3.38 (dd, $^3J_{HH}$ = 11 Hz, 1H, C_2H_4), 2.67 (dd, $^3J_{HH}$ = 11 Hz, 1H, C_2H_4), 2.46 (s, 3H, CH_3), 2.40 (s, 3H, CH_3), 2.05 (dd, $^3J_{HH}$ = 11 Hz, 1H, C_2H_4), 1.81 (dd, $^3J_{HH}$ = 11 Hz, 1H, C_2H_4). $^{13}C\{^1H\}$ NMR (201 MHz, CD_2Cl_2, 25 °C): δ 151.7, 149.8, 148.5, 144.9, 140.7, 139.5, 133.2, 133.0, 132.5, 131.2, 129.8, 128.7, 122.1, 121.4, 117.3, 116.8, 102.6, 102.4, 20.0 (two CH_3). Note: the peak for C_2H_4 is too broad to observe in the $^{13}C\{^1H\}$ NMR spectrum at room temperature. ^1H NMR spectrum at −60 °C can be found in Figure S62. Acceptable elemental analysis results for **3a** could not be obtained. The NMR spectra of **3a** appear in Figures S6-S9.

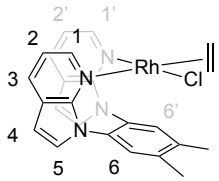

(6-^{Me}FP)Rh(C_2H_4)Cl (6a). In a round bottom flask, a THF solution (10 mL) of 6-^{Me}FP (77 mg, 214 μmol) was added to a THF solution (20 mL) of $[Rh(C_2H_4)_2(\mu\text{-}Cl)]_2$ (42 mg, 107 μmol). The reaction mixture was allowed to stir overnight, during which time the solution turned from orange to dark red. The solvent was removed under vacuum to give a red solid. The crude solid was dissolved in a minimal amount of methylene chloride, and 50 mL of cold (−30 °C) *n*-pentane were added to precipitate a red solid, which was then dried under vacuum. The isolated yield was 74% (83 mg). See below for structure and assignments. ^1H NMR (600 MHz, C_6D_6): δ 9.93 (d, $^3J_{HH}$ = 5 Hz, 1H, *1* or *1*' position), 8.20 (d, $^3J_{HH}$ = 5 Hz, 1H, *1* or *1*' position), 7.80 (s, 1H, *7* or *7*' position), 7.50 (d, $^3J_{HH}$ = 7 Hz, 1H, *3* or *3*' position), 7.18 (m, 2H, *3* or *3*', *7* or *7*' position), 7.03 (d, $^3J_{HH}$ = 7 Hz, 1H, *4*, *4*', *6* or *6*' position), 6.87 (t, $^3J_{HH}$ = 8 Hz, 1H,

5 or *5*’ position), 6.84 (d, $^3J_{HH}$ = 8 Hz, 1H, *4*, *4*’, *6* or *6*’ position), 6.75 (d, $^3J_{HH}$ = 8 Hz, 1H, *4*, *4*’, *6* or *6*’ position), 6.71 (d, $^3J_{HH}$ = 8 Hz, 1H, *4*, *4*’, *6* or *6*’ position), 6.65 (dd, $^3J_{HH}$ = 8, 5 Hz, 1H, *2* or *2*’ position), 6.62 (t, $^3J_{HH}$ = 8 Hz, 1H, *5* or *5*’ position), 5.79 (dd, $^3J_{HH}$ = 8, 5 Hz, 1H, *2* or *2*’ position), 4.46 (br, 1H, C_2H_4), 2.76 (br, 1H, C_2H_4), 2.51 (s and br, 4H, CH_3, C_2H_4), 2.45 (s, 3H, CH_3), 1.98 (br, 1H, C_2H_4). $^{13}C\{^1H\}$ NMR (201 MHz, CD_2Cl_2): δ 155.0, 154.4, 151.2, 149.1, 141.6, 140.7, 137.2, 136.8, 136.4, 135.5, 134.9, 133.8, 131.8, 130.0, 129.2, 129.2, 128.9, 127.8, 127.5, 127.4, 127.0, 126.5, 121.5, 121.5, 44.2 (C_2H_4), 34.0 (C_2H_4), 20.2 (CH_3), 20.0 (CH_3). Anal. Calcd. for $C_{28}H_{24}N_2RhCl$: C, 63.83; H, 4.59; N, 5.32. Found: C, 63.40; H, 4.53; N, 4.95.

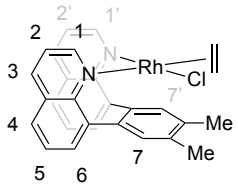

[(5-FP)Ir(COD)][IrCl$_2$(COD)] (1b). In a pressure tube, a THF solution (5 mL) of 5-FP (29.1 mg, 93.8 μmol) was added to a THF solution (10 mL) of [Ir(COE)$_2$(μ-Cl)]$_2$ (84.0 mg, 93.8 μmol) in the glovebox and sealed. The pressure tube was brought outside of the glovebox and heated at 70 °C in an oil bath with stirring for 24 h. During this time, the solution turned from yellow to brown. The reaction mixture was allowed to cool to room temperature and taken into the glovebox. THF was removed under vacuum, and the resulting solid was dissolved in a minimal amount of methylene chloride, followed by addition of pentane to precipitate the product. The product was collected via filtration through a fine porosity frit, pentane was used to wash the yellow product, and the solid was dried under vacuum. The isolated yield was 82% (75.4 mg). See below for structure and assignments. ^1H NMR (497 MHz, CD_2Cl_2): δ 8.52 (d, $^3J_{HH}$ = 5 Hz, 2H, *1* position), 7.99 (dd, 2H, *6* or *7* position), 7.92 (d, $^3J_{HH}$ = 8 Hz, 2H, position *3*), 7.68 (dd, 2H, *6* or *7* position), 7.22 (d, $^3J_{HH}$ = 3 Hz, 2H, *4* or *5* position), 7.18 (d, $^3J_{HH}$ = 7 Hz, 2H, *2* position), 6.63

(d, $^3J_{HH}$ = 3 Hz, 2H, *4* or *5* position), 3.88 (m, 2H, COD), 3.77 (m, 2H, COD), 3.33 (m, 2H, COD), 2.42 (m, 2H, COD), 2.13 (m, 2H, COD), 1.71 – 1.62 (m, 4H, COD), 1.54 (s, 8H, COD). $^{13}C\{^1H\}$ NMR (151 MHz, CD_2Cl_2): δ 149.1, 143.6, 136.9, 132.6, 132.5, 132.3, 131.1, 124.6, 118.6, 104.5, 74.2 (COD), 65.2 (COD), 31.7 (COD), 30.1 (COD). Acceptable elemental analysis results for **1b** could not be obtained. The NMR spectra of **3a** appear in Figures S14-S15.

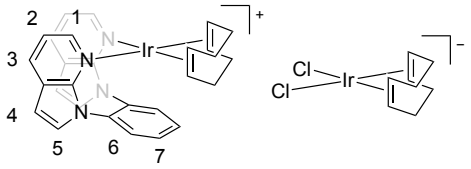

[(5-FP)Ir(C_2H_4)$_2$][IrCl_2(C_2H_4)$_2$] (1d). In a round bottom flask, a THF solution (10 mL) of 5-FP (41.6 mg, 129 μmol) was added to a THF solution (20 mL) of [Ir(C_2H_4)$_2$(μ-Cl)]$_2$ (73.3 mg, 129 μmol). The reaction mixture was allowed to stir for 2 h. During this time the solution turned from red to brown. The solvent was removed under vacuum to give a dark brown solid. The solid was dissolved in a minimal amount of methylene chloride, and 50 mL of pentane were added to precipitate a yellow solid, which was dried under vacuum. The isolated yield was 75% (85.0 mg). See below for structure and assignments. ^1H NMR (598 MHz, CD_3OD): δ 8.60 (d, $^3J_{HH}$ = 6 Hz, 2H, *1* position), 8.03 (m, 2H, *6* or *7* position), 8.01 (m, 2H, *3* position), 7.95 (m, 2H, *6* or *7* position), 7.50 (d, $^3J_{HH}$ = 4 Hz, 2H, *4* or *5* position), 7.23 (m, 2H, *2* position), 6.70 (d, $^3J_{HH}$ = 4 Hz, 2H, *4* or *5* position), 3.73 (br, 4H, C_2H_4), 2.75 (m, 4H, C_2H_4), 2.55 (m, 4H, C_2H_4), 1.87 (br, 4H, C_2H_4). $^{13}C\{^1H\}$ NMR (201 MHz, CD_2Cl_2): δ 148.8, 142.7, 136.3, 132.8, 132.4, 132.2, 131.9, 124.8, 119.0, 104.6, 54.9 ([(5-FP)Ir(C_2H_4)$_2$]$^+$), 40.4 ([IrCl_2(C_2H_4)$_2$]$^-$). Anal. Calcd. for $C_{28}H_{30}N_4Ir_2Cl_2$: C, 38.31; H, 3.44; N, 6.38. Found: C, 38.45; H, 3.37; N, 6.14.

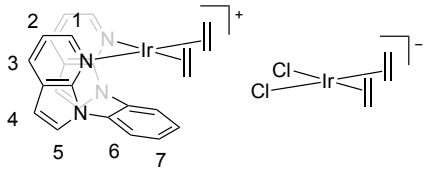

[(5-^{Me}FP)Ir(C_2H_4)$_2$][IrCl_2(C_2H_4)$_2$] (3d). In a round bottom flask, a THF solution (10 mL) of 5-^{Me}FP (30.0 mg, 89 μmol) was added to a THF solution (20 mL) of [Ir(C_2H_4)$_2$(μ-Cl)]$_2$ (51.1 mg, 89 μmol). The reaction mixture was allowed to stir for 2 h, during which time the solution turned from red to brown. The solvent was removed under vacuum to give a dark brown solid. The crude solid was dissolved in a minimal amount of methylene chloride, and 50 mL of pentane were added to precipitate a yellow solid, which was dried under vacuum. The isolated yield was 68% (54.8 mg). See below for structure and assignments. ^{1}H NMR (600 MHz, CD_2Cl_2): δ 8.52 (d, $^3J_{HH}$ = 6 Hz, 2H, *1* position), 7.94 (d, $^3J_{HH}$ = 8 Hz, 2H, *3* position), 7.52 (s, 2H, *6* position), 7.28 (d, $^3J_{HH}$ = 4 Hz, 2H, *4* or *5* position), 7.22 (dd, $^3J_{HH}$ = 8, 6 Hz, 2H, *2* position), 6.65 (d, $^3J_{HH}$ = 4 Hz, 2H, *4* or *5* position), 3.22 (s, 4H, C_2H_4), 2.66 (m, 4H, C_2H_4), 2.53 (s, 6H, CH_3), 2.48 (m, 4H, C_2H_4), 1.63 (m, 4H, C_2H_4). ^{13}C{^{1}H} NMR (201 MHz, CD_2Cl_2): δ 148.2, 142.1, 141.4, 132.6, 132.1, 131.8, 131.6, 124.2, 118.2, 103.8, 53.5 (C_2H_4), 39.81 (C_2H_4), 19.56 (CH_3). Acceptable elemental analysis results for **3d** could not be obtained. The NMR spectra of **3d** appear in Figures S19-S22.

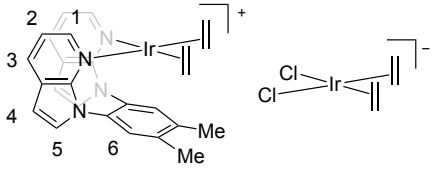

[(5-FP)Ir(C_2H_4)$_2$][BF_4] (1e-BF_4). In a round bottom flask, a THF solution (15 mL) of 5-FP (50.0 mg, 161 μmol) was added to a THF solution (30 mL) of [Ir(C_2H_4)$_2$(μ-Cl)]$_2$ (45.7 mg, 80.5 μmol). The reaction mixture was allowed to stir for 2 h, during which time the solution turned from red to brown. $AgBF_4$ (31.4

mg, 161 μmol) was added to the solution, and the reaction mixture was stirred overnight in the dark. The resulting suspension was filtered through a Celite-loaded fine porosity frit. The solvent was removed from the filtrate under vacuum to give a dark brown solid. The solid was dissolved in a minimal amount of methylene chloride, and 50 mL of pentane were added to precipitate a yellow product, which was dried under vacuum. The isolated yield was 72% (75.2 mg). See below for structure and assignments. ^{1}H NMR (800 MHz, CD_2Cl_2): δ 8.46 (dd, $^{3}J_{HH}$ = 6 Hz, $^{4}J_{HH}$ = 1 Hz, 2H, *1* position), 7.97 (dd, *J* = 6, 4 Hz, 2H, *6* or *7* position), 7.95 (dd, $^{3}J_{HH}$ = 8, $^{4}J_{HH}$ = 1 Hz, 2H, *3* position), 7.78 (dd, $^{3}J_{HH}$ = 6, 4 Hz, 2H, *6* or *7* position), 7.29 (d, $^{3}J_{HH}$ = 4 Hz, 2H, *4* or *5* position), 7.21 (dd, $^{3}J_{HH}$ = 8, 6 Hz, 2H, *2* position), 6.68 (d, $^{3}J_{HH}$ = 4 Hz, 2H, *4* or *5* position), 2.70 – 2.65 (m, 4H, C_2H_4), 2.51 – 2.49 (m, 4H, C_2H_4). ^{13}C{^{1}H} NMR (201 MHz, CD_2Cl_2): δ 148.3, 141.8, 135.7, 132.3, 131.8, 131.6, 131.3, 124.3, 118.3, 104.1, 54.3. ^{19}F NMR (564 MHz, CD_2Cl_2): δ -151.4 (s, 20%, $^{10}BF_4^-$), -151.4 (s, 80%, $^{11}BF_4^-$). Anal. Calcd. for $C_{24}H_{22}N_4IrBF_4$: C, 44.66; H, 3.44; N, 8.68. Found: C, 43.86; H, 3.32; N, 8.58.

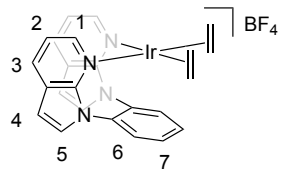

[(5-^{Me}FP)Ir(C_2H_4)$_2$][BF_4] (3e-BF_4). In a round bottom flask, a THF solution (20 mL) of 5-^{Me}FP (115 mg, 339 μmol) was added to a THF solution (30 mL) of [Ir(C_2H_4)$_2$(μ-Cl)]$_2$ (96 mg, 169 μmol). The reaction mixture quickly turned from red to orange. $AgBF_4$ (66 mg, 339 μmol) was then added to the solution, and the reaction mixture was stirred for 24 h in the dark. The resulting suspension was filtered through a Celite-loaded frit with fine porosity. The solvent was removed from the filtrate under vacuum to give an orange solid. The solid was dissolved in a minimal amount of methylene chloride (2 mL), and 70 mL of cold *n*-pentane (−30 °C) was added to precipitate the orange product, which was then dried under

vacuum. The isolated yield was 88% (200 mg). See below for structure and assignments. ^{1}H NMR (800 MHz, CD_2Cl_2): δ 8.46 (dd, $^{3}J_{HH}$ = 6 Hz, $^{4}J_{HH}$ = 1 Hz, 2H, *1* position), 7.94 (dd, $^{3}J_{HH}$ = 8 Hz, $^{4}J_{HH}$ = 1 Hz, 2H, *3* position), 7.52 (s, 2H, *6* position), 7.25 (d, $^{3}J_{HH}$ = 4 Hz, 2H, *4* or *5* position), 7.20 (dd, $^{3}J_{HH}$ = 6, 8 Hz, 2H, *2* position), 6.65 (d, $^{3}J_{HH}$ = 4 Hz, 2H, *4* or *5* position), 2.67 – 2.64 (m, 4H, C_2H_4), 2.53 (s, 6H, CH_3), 2.49 – 2.45 (m, 4H, C_2H_4). ^{13}C{1H} NMR (201 MHz, CD_2Cl_2): δ 148.8, 142.4, 142.0, 133.2, 132.7, 132.4, 132.2, 124.8, 118.7, 104.3, 54.2 (C_2H_4), 20.1 (CH_3). ^{19}F NMR (564 MHz, CD_2Cl_2): δ -151.58 (s, 20%, BF_4^-), -151.63 (s, 80%, BF_4^-). Anal. Calcd. for $C_{26}H_{26}N_4IrBF_4$: C, 46.36; H, 3.89; N, 8.32. Found: C, 46.56; H, 4.12; N, 7.95.

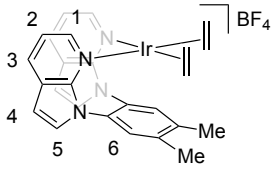

(5-^{NP}FP)Ir(COE)Cl (2f). In a 20 mL vial, a THF (5 mL) solution of 5-^{NP}FP (50.0 mg, 139 μmol) was added dropwise to a THF (10 mL) solution of $[Ir(COE)_2(\mu\text{-}Cl)]_2$ (62.1 mg, 69 μmol). The reaction mixture, which quickly turned from yellow to orange, was allowed to stir overnight. THF was removed under vacuum. The product was dissolved in a minimal amount of methylene chloride, and then 20 mL of *n*-pentane were added to precipitate a yellow solid. The product was dried under vacuum. The isolated yield was 65% (62.5 mg). See below for structure and assignments. ^{1}H NMR (600 MHz, THF-d_8): δ 8.34 (dd, $^{3}J_{HH}$ = 5 Hz, $^{4}J_{HH}$ = 1 Hz, 1H, *1* or *1*' position), 8.10 (d, $^{3}J_{HH}$ = 4 Hz, 1H, *4*, *4*', *5* or *5*' position), 7.95 (d, $^{3}J_{HH}$ = 6 Hz, 1H, *1* or *1*' position), 7.94 – 7.92 (m, 1H, *7*, *7*', *8* or *8*' position), 7.69 (d, $^{3}J_{HH}$ = 8 Hz, 1H, *7*, *7*', *8* or *8*' position), 7.65 (d, $^{3}J_{HH}$ = 8 Hz, 1H, *3* or *3*' position), 7.43 (d, $^{3}J_{HH}$ = 8 Hz, 1H, *3* or *3*' position), 7.28 (dd, $^{3}J_{HH}$ = 7 Hz, 1H, *7*, *7*', *8* or *8*' position), 7.22 (d, $^{3}J_{HH}$ = 3 Hz, 1H, 1H, *4*, *4*', *5* or *5*' position), 7.12 (dd, $^{3}J_{HH}$ = 7 Hz, 1H, *7*, *7*', *8* or *8*' position), 7.04 (dd, $^{3}J_{HH}$ = 8, 6 Hz, 1H, *2* or *2*' position), 6.93 (s, 1H, *6*

or *6*' position), 6.90 (dd, $^3J_{HH}$ = 8, 5 Hz, 1H, *2* or *2*' position), 6.71 (d, $^3J_{HH}$ = 4 Hz, 1H, *4*, *4*', *5* or *5*' position), 6.46 (d, $^3J_{HH}$ = 3 Hz, 1H, *4*, *4*', *5* or *5*' position), 6.44 (s, 1H, *6* or *6*' position), 4.73 (t, $^3J_{HH}$ = 10 Hz, 1H, COE), 3.34 (t, $^3J_{HH}$ = 10 Hz, 1H, COE), 2.62 (m, 1H, COE), 2.22 – 2.16 (m, 1H, COE), 2.16 – 2.11 (m, 1H, COE), 2.02 – 1.81 (m, 3H, COE), 1.68 – 1.45 (m, 4H, COE), 1.37 (m, 2H, COE). $^{13}C\{^1H\}$ NMR (201 MHz, CD_2Cl_2): δ 156.6, 149.6, 142.8, 139.0, 137.4, 133.3, 131.3, 130.0, 128.8, 128.3, 128.2, 127.5, 127.4, 126.4, 124.6, 122.8, 118.5, 118.4, 118.4, 117.3, 104.5, 102.4, 77.3, 58.4, 48.6, 47.5, 33.3, 31.5, 29.5, 27.5, 27.4. Anal. Calcd. for $C_{32}H_{30}N_4IrCl$: C, 55.04; H, 4.33; N, 8.02. Found: C, 54.77; H, 4.60; N, 7.60.

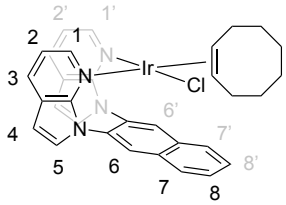

(6-^{NP}FP)Ir(COE)Cl (5f). In a 20 mL vial, a THF (5 mL) solution of 6-^{NP}FP (37 mg, 96 μmol) was added dropwise to a THF (10 mL) solution of $[Ir(COE)_2(\mu\text{-}Cl)]_2$ (43 mg, 48 μmol), and the reaction mixture quickly turned from orange to red. The solution stirred for 6 h. THF was removed under vacuum. The product was dissolved in a minimal amount of methylene chloride, and then 20 mL of *n*-pentane were added to precipitate a bright red solid. The product was dried under vacuum. The isolated yield was 81% (56 mg). See below for structure and assignments. ^1H NMR (800 MHz, C_6D_6): δ 8.98 (d, $^3J_{HH}$ = 5 Hz, 1H, 3 or 3' position), 8.22 (d, $^3J_{HH}$ = 6 Hz, 1H, 3 or 3' position), 8.18 (d, $^3J_{HH}$ = 8 Hz, 1H, 3, 3', 4 or 4' position), 7.89 (d, $^3J_{HH}$ = 8 Hz, 1H, 3, 3', 4 or 4' position), 7.68 (d, $^3J_{HH}$ = 8 Hz, 1H, 3, 3', 4 or 4' position), 7.50 (s, 1H, 7 or 7' position), 7.41 (t, $^3J_{HH}$ = 8 Hz, 1H, 5 or 5' position), 7.28 (t, $^3J_{HH}$ = 8 Hz, 1H, 5 or 5' position), 7.24 (d, $^3J_{HH}$ = 8 Hz, 1H, 3, 3', 4 or 4' position), 7.08 (m, 1H, 8, 8' 9 or 9 position), 7.07 (m, 1H, 8, 8' 9 or 9 position), 6.99 (m, 1H, 1 or 1' position), 6.98 (m, 1H, 2 or 2' position), 6.52 (m, 1H, 8, 8' 9 or

9 position), 6.51 (m, 1H, m, 1H, 8, 8' 9 or 9 position), 6.39 (dd, $^3J_{HH}$ = 8, 6 Hz, 1H, 2 or 2' position), 6.29 (s, 1H, 7 or 7' position), 6.02 (dd, $^3J_{HH}$ = 8, 5 Hz, 1H, 2 or 2'), 4.86 (ddd, *J* = 12, 9, 3 Hz, 1H, COE, 10 or 17), 3.27 (m, 1H, COE, 16 or 11), 2.60 (dq, *J* = 15, 3 Hz, 1H, COE, 16 or 11), 2.51 (m, 1H, COE, 11 or 16), 2.35 (ddd, *J* = 11, 8, 3 Hz, 1H, COE, 17 or 10), 2.19 (m, 1H, COE, 15 or 12), 2.16 (m, 1H, COE, 13 or 14), 2.14 (m, 1H, COE, 11 or 16), 2.08 (ddd, *J* = 12, 9, 4 Hz, 1H, COE, 13 or 14), 2.01 (m, 1H, COE, 12 or 15), 1.93 (m, 1H, COE, 15 or 12), 1.92 (m, 1H, COE, 12 or 15), 1.81 (td, *J* = 13, 12, 6 Hz, 1H, COE, 14 or 13), 1.62 (dtd, *J* = 12, 9, 3 Hz, 1H, COE, 14 or 13). $^{13}C\{^1H\}$ NMR (201 MHz, C_6D_6): δ 158.5, 155.6, 145.6, 145.1, 141.2, 140.7, 137.9, 137.8, 134.6, 132.9, 129.8, 129.7, 129.6, 129.5, 128.4, 128.2, 128.0, 127.0, 126.8, 126.7, 124.3, 123.2, 121.5, 121.4, 120.8, 120.7, 74.5, 60.6, 59.2, 46.8, 33.5, 31.1, 29.0, 28.1, 27.4, 27.3. Anal. Calcd. for $C_{36}H_{32}N_2IrCl$: C, 60.03; H, 4.48; N, 3.89. Found: C, 59.29; H, 4.48; N, 3.46.

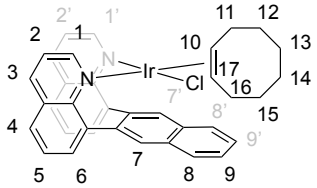

(5-^{NP}FP)Ir(C_2H_4)Cl (2h). In the glovebox, (5-^{NP}FP)Ir(COE)Cl (178 mg, 255 μmol) was dissolved in DCM (10 mL) in a Fisher-Porter tube which was sealed and brought out of the glovebox. Ethylene (50 psig) was charged into the Fisher-Porter tube. The solution stirred at room temperature for 2 h. The reaction was vented while purging with N_2 and cold *n*-pentane was added (50 mL). The reactor was recharged with ethylene (50 psig) and placed in the freezer. After 30 m, the reaction was vented. The solution was filtered through a frit with fine porosity, brought into the glovebox and dried. The isolated yield was 73% (115 mg). See below for structure and assignments. ^1H NMR (600 MHz, THF-d_8): δ 8.44 (dd, $^3J_{HH}$ = 5 Hz, $^4J_{HH}$ = 1 Hz, 1H, *1* or *1*' position), 8.11 (d, $^3J_{HH}$ = 4 Hz, 1H, *4*, *4*', *5* or *5*' position), 8.00

(d, $^3J_{HH}$ = 6 Hz, 1H, *1* or *1*' position), 7.94 (dd, $^3J_{HH}$ = 8 Hz, $^4J_{HH}$ = 1 Hz, 1H, *3* or *3*' position), 7.646 (d, $^3J_{HH}$ = 8 Hz, 1H, *3* or *3*' position), 7.62 (d, $^3J_{HH}$ = 8 Hz, 1H, *7*, *7*', *8* or *8*' position), 7.66 (d, $^3J_{HH}$ = 8 Hz, 1H), 7.29 – 7.24 (m, 2H, two of *7*, *7*', *8* or *8*' position), 7.15 – 7.11 (m, 1H, *7*, *7*', *8* or *8*' position), 6.98 (dd, $^3J_{HH}$ = 8, 6 Hz, 1H, *2* or *2*' position), 6.93 (s, 1H, *6* or *6*' position), 6.87 (dd, $^3J_{HH}$ = 8, 5 Hz, 1H, *2* or *2*' position), 6.72 (d, $^3J_{HH}$ = 4 Hz, 1H, *4*, *4*', *5* or *5*' position), 6.50 (d, $^3J_{HH}$ = 3 Hz, 1H, *4*, *4*', *5* or *5*' position), 6.45 (s, 1H, *6* or *6*' position), 4.02 (t, $^3J_{HH}$ = 9 Hz, 1H, C_2H_4), 3.75 (t, $^3J_{HH}$ = 9 Hz, 1H, C_2H_4), 3.55 (t, $^3J_{HH}$ = 9 Hz, 1H, C_2H_4), 2.89 (t, $^3J_{HH}$ = 9 Hz, 1H, C_2H_4). $^{13}C\{^1H\}$ NMR (201 MHz, CD_2Cl_2): δ 156.9, 150.9, 144.0, 142.8, 139.2, 139.0, 133.1, 131.5, 130.6, 130.1, 128.4, 128.3, 128.2, 127.6, 126.5, 125.1, 122.7, 118.5, 118.5, 118.5, 117.6, 117.0, 104.8, 102.5, 38.0 (C_2H_4), 29.8 (C_2H_4). Acceptable elemental analysis results for **2h** could not be obtained. The NMR spectra of **2h** appear in Figures S37 and S38.

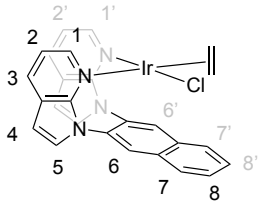

(6-FP)Ir(C_2H_4)Cl (4h). In a 100 mL round bottom flask, a THF (15 mL) solution of 6-FP (70.3 mg, 211 μmol) was added dropwise to a THF (30 mL) solution of $[Ir(C_2H_4)_2(\mu\text{-}Cl)]_2$ (60.0 mg, 106 μmol). The reaction mixture quickly turned from orange to dark red. The mixture was stirred for 12 h. THF was removed under vacuum. The product was dissolved in 3 mL of methylene chloride, and then 70 mL of *n*-pentane were added to give a dark red precipitate. The solid was collected and dried under reduced pressure. The isolated yield was 90% (112.2 mg). See below for structure and assignments. ^1H NMR (600 MHz, CD_2Cl_2): δ 9.42 (dd, $^3J_{HH}$ = 5 Hz, $^4J_{HH}$ = 2 Hz, 1H, *1* or *1*' position), 8.31 (dd, $^3J_{HH}$ = 5 Hz, $^4J_{HH}$ = 1 Hz, 1H, *1* or *1*' position), 8.14 (dd, $^3J_{HH}$ = 8 Hz, $^4J_{HH}$ = 2 Hz, 1H, *3* or *3*' position), 7.80 (dd, $^3J_{HH}$ = 8 Hz, $^4J_{HH}$ = 1 Hz, 1H, *3* or *3*' position), 7.57 (m, 2H, *4*, *4*', *6* or *6*'; *7*, *7*', *8* or *8*' position), 7.44 (dd, $^3J_{HH}$ = 8

Hz, $^4J_{HH}$ = 1 Hz, 1H, *4*, *4*', *6* or *6*' position), 7.39 – 7.34 (m, 2H, *7*, *7*', *8* or *8*'; *5* or *5*' position), 7.31 (dd, $^3J_{HH}$ = 8, 5 Hz, 1H, *2* or *2*' position), 7.25 (dd, $^3J_{HH}$ = 8, 7 Hz, 1H, *5* or *5*' position), 7.18 (dd, $^3J_{HH}$ = 8 Hz, $^4J_{HH}$ = 1 Hz, 1H, *4*, *4*', *6* or *6*' position), 7.14 (dd, $^3J_{HH}$ = 8 Hz, 1H, *7*, *7*', *8* or *8*' position), 7.05 (dd, $^3J_{HH}$ = 8 Hz, 1H, *7*, *7*', *8* or *8*' position), 6.86 – 6.80 (m, 2H, *2* and *2*' position), 3.20 (ddd, $^3J_{HH}$ = 10, 9 Hz, $^4J_{HH}$ = 1 Hz, 1H, C_2H_4), 2.65 (ddd, $^3J_{HH}$ = 9, 9 Hz, $^4J_{HH}$ = 2 Hz, 1H, C_2H_4), 2.34 (ddd, $^3J_{HH}$ = 10, 8 Hz, $^4J_{HH}$ = 2 Hz, 1H, C_2H_4), 1.78 – 1.72 (m, 1H, C_2H_4). $^{13}C\{^1H\}$ NMR (201 MHz, CD_2Cl_2): δ 156.7, 155.8, 151.4, 150.0, 145.5, 142.1, 136.9, 134.3, 132.6, 132.4, 131.6, 130.3, 129.7, 128.4, 127.5, 127.3, 126.1, 125.9, 123.6, 123.1, 122.2, 117.3, 112.7, 94.9, 30.6 (C_2H_4), 17.8 (C_2H_4). Anal. Calcd. for $C_{26}H_{20}N_2ClIr$: C, 53.10; H, 3.43; N, 4.76. Found: C, 52.66; H, 3.66; N, 4.32.

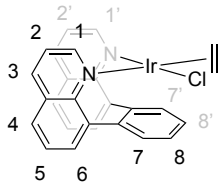

(6-^{NP}FP)Ir(C_2H_4)Cl (5h). In a round bottom flask, a THF (10 mL) solution of 6-^{NP}FP (55.8 mg, 146 μmol) was added dropwise to a THF (20 mL) solution of $[Ir(C_2H_4)_2(\mu\text{-}Cl)]_2$ (41.4 mg, 73 μmol). The reaction mixture was allowed to stir for 3 h. Then, THF was removed under vacuum. The crude solid was dissolved in a minimal amount of methylene chloride, and then 30 mL of *n*-pentane were added, and a bright red precipitate formed. The product was dried under vacuum. The isolated yield was 85% (79.1 mg). See below for structure and assignments. ^1H NMR (800 MHz, C_6D_6): δ 9.12 (d, $^3J_{HH}$ = 5 Hz, 1H, *1* or *1*' position), 8.20 (d, $^3J_{HH}$ = 6 Hz, 1H, *1* or *1*' position), 8.18 (d, $^3J_{HH}$ = 7 Hz, 1H, *4*, *4*', *6* or *6*' position), 7.83 (d, $^3J_{HH}$ = 8 Hz, 1H, *4*, *4*', *6* or *6*' position), 7.70 (d, $^3J_{HH}$ = 8 Hz, 1H, *4*, *4*', *6* or *6*' position), 7.45 (s, 1H, *7* or *7*' position), 7.40 (d, $^3J_{HH}$ = 7 Hz, 1H, *4*, *4*', *6* or *6*' position), 7.30 (dd, $^3J_{HH}$ = 7, 7 Hz, 1H, *5* or *5*' position), 7.24 (dd, $^3J_{HH}$ = 8 Hz, 1H, *8*, *8*', *9* or *9*' position), 7.10 (m, 1H, *8*, *8*', *9* or *9*' position),

7.09 – 7.08 (m, 1H, *8*, *8*', *9* or *9*' position), 7.03 (dd, $^{3}J_{HH}$ = 8 Hz, $^{4}J_{HH}$ = 2 Hz, 1H, *3* or *3*' position), 6.98 (dd, $^{3}J_{HH}$ = 8 Hz, $^{4}J_{HH}$ = 1 Hz, 1H, *3* or *3*' position), 6.55 – 6.52 (m, 2H, *5* or *5*', *8*, *8*', *9* or *9*' position), 6.31 (dd, $^{3}J_{HH}$ = 9, 5 Hz, 1H, *2* or *2*' position), 6.27 (s, 1H, *7* or *7*' position), 6.02 (dd, $^{3}J_{HH}$ = 8, 5 Hz, 1H, *2* or *2*' position), 4.61 (ddd, $^{3}J_{HH}$ = 9, 9 Hz, $^{4}J_{HH}$ = 2 Hz, 1H), 4.34 (dd, $^{3}J_{HH}$ = 10, 8 Hz, 1H), 4.16 (ddd, $^{3}J_{HH}$ = 10, 8 Hz, $^{4}J_{HH}$ = 2 Hz, 1H), 2.05 (dd, $^{3}J_{HH}$ = 9, 9 Hz, 1H). $^{13}C\{^{1}H\}$ NMR (201 MHz, C_6D_6) δ 160.0, 155.7, 146.3, 145.5, 141.4, 140.8, 138.0, 137.8, 134.4, 132.8, 129.9, 129.8, 129.6, 129.6, 129.5, 128.5, 128.0, 127.9, 127.2, 126.9, 126.8, 126.0, 124.7, 123.3, 121.9, 120.8, 74.8, 60.5, 40.8 (C_2H_4), 29.5 (C_2H_4). Anal. Calcd. for $C_{30}H_{22}N_2ClIr$: C, 56.46; H, 3.47; N, 4.39. Found: C, 56.54; H, 3.53; N, 4.33.

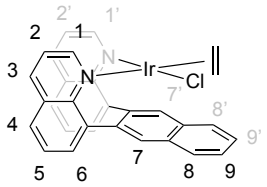

(6-^{Me}FP)Ir(C_2H_4)Cl (6h). In a 100 mL round bottom flask, a THF (10 mL) solution of 6-^{Me}FP (60.0 mg, 166 μmol) was added dropwise to a THF (20 mL) solution of $[Ir(C_2H_4)_2(\mu\text{-}Cl)]_2$ (47.2 mg, 83 μmol). The reaction mixture quickly turned from orange to dark red. The mixture was stirred for 10 h. Then, THF was removed under vacuum. The crude product was dissolved in 2 mL of methylene chloride, and then 50 mL of *n*-pentane were added to give a dark red precipitate. The solid was dried in vacuo and isolated in 90% yield (92.0 mg). See below for structure and assignments. ^{1}H NMR (600 MHz, C_6D_6): δ 9.28 (dd, $^{3}J_{HH}$ = 5 Hz, $^{4}J_{HH}$ = 2 Hz, 1H, *1* or *1*' position), 8.10 (d, $^{3}J_{HH}$ = 5 Hz, 1H, *1* or *1*' position), 7.48 (dd, $^{3}J_{HH}$ = 7 Hz, $^{4}J_{HH}$ = 1 Hz, 1H, *4*, *4*', *6* or *6*' position), 7.35 (dd, $^{3}J_{HH}$ = 7 Hz, $^{4}J_{HH}$ = 1 Hz, 1H, *4*, *4*', *6* or *6*' position), 7.15 (m, 1H, *3* or *3*' position), 7.00 (s, 1H, *7* or *7*' position), 6.95 (d, $^{3}J_{HH}$ = 8 Hz, 1H, *4*, *4*', *6* or *6*' position), 6.88 (s, 1H, *7* or *7*' position), 6.88 – 6.85 (m, 2H, *3* or *3*', *5* or *5*' position), 6.69 (dd, $^{3}J_{HH}$ = 8, 7 Hz, 1H, *5* or *5*' position), 6.66 (dd, $^{3}J_{HH}$ = 8 Hz, $^{4}J_{HH}$ = 1 Hz, 1H, *4*, *4*', *6* or *6*' position), 6.29 (dd,

$^3J_{HH}$ = 8, 5 Hz, 1H, *2* or *2*' position), 5.96 (dd, $^3J_{HH}$ = 8, 5 Hz, 1H, *2* or *2*' position), 4.25 (dd, $^3J_{HH}$ = 9 Hz, 1H, C_2H_4), 4.04 (dd, $^3J_{HH}$ = 9 Hz, 1H, C_2H_4), 3.10 (dd, $^3J_{HH}$ = 9 Hz, 1H, C_2H_4), 2.43 (s, 3H, CH_3), 2.41 (s, 3H, CH_3), 1.93 (dd, $^3J_{HH}$ = 9 Hz, 1H, C_2H_4). $^{13}C\{^1H\}$ NMR (201 MHz, C_6D_6): δ 157.4, 156.4, 149.5, 147.4, 146.0, 142.3, 136.0, 135.3, 133.6, 132.9, 132.3, 131.3, 130.3, 129.8, 129.7, 127.6, 126.9, 126.7, 124.8, 122.4, 121.2, 119.1, 104.1, 93.0, 31.9 (C_2H_4), 19.9 (CH_3), 19.6 (CH_3), 19.5 (C_2H_4). Anal. Calcd. for $C_{28}H_{24}N_2IrCl$: C, 54.58; H, 3.93; N, 4.55. Found: C, 54.49; H, 4.06; N, 4.45.

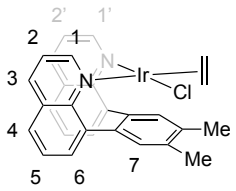

(6-^{F}FP)Ir(C_2H_4)Cl (7h). In a 100 mL round bottom flask, a THF (10 mL) solution of 6-^{F}FP (51.0 mg, 138 μmol) was added dropwise to a THF (20 mL) solution of $[Ir(C_2H_4)_2(\mu\text{-}Cl)]_2$ (39.3 mg, 69 μmol). The reaction mixture quickly turned from orange to dark red, and then the solution was allowed to stir for 10 h. Next, THF was removed under vacuum. The resulting solid was dissolved in 2 mL of methylene chloride, and then 80 mL of *n*-pentane were added to form a reddish orange precipitate. The solid was isolated and dried in vacuo to give 97% yield (83.2 mg). See below for structure and assignments. ^1H NMR (800 MHz, CD_2Cl_2): δ 9.34 (d, $^3J_{HH}$ = 5 Hz, 1H, *1* or *1*' position), 8.33 (d, $^3J_{HH}$ = 5 Hz, 1H, *1* or *1*' position), 8.13 (d, $^3J_{HH}$ = 8 Hz, 1H, *3* or *3*' position), 7.87 (d, $^3J_{HH}$ = 8 Hz, 1H, *3* or *3*' position), 7.69 (d, $^3J_{HH}$ = 7 Hz, 1H, one of *4*, *4*', *6*, *6*' position), 7.66 (d, $^3J_{HH}$ = 8 Hz, 1H, one of *4*, *4*', *6*, *6*' position), 7.47 (d, $^3J_{HH}$ = 8 Hz, 1H, one of *4*, *4*', *6*, *6*' position), 7.44 – 7.39 (m, 2H, *5* or *5*', and one of *4*, *4*', *6*, *6*' position), 7.30 (m, 1H, *5* or *5*' position), 7.24 (dd, $^3J_{HH}$ = 8, $^3J_{HH}$ = 5 Hz, 1H, *2* or *2*' position), 7.01 (dd, $^3J_{HH}$ = 8, 6 Hz, $^3J_{HH}$ = 1H, *2* or *2*' position), 6.68 (dd, $^3J_{HF}$ = 10 Hz, $^4J_{HF}$ = 8 Hz, 1H, *7* position), 6.52 (dd, $^3J_{HF}$ = 11 Hz, $^4J_{HF}$ = 8 Hz, 1H, *7*' position), 3.44 (dd, $^3J_{HH}$ = 9 Hz, 1H, C_2H_4), 3.37 (dd, $^3J_{HH}$ = 9 Hz, 1H, C_2H_4), 2.98

(dd, $^{3}J_{HH}$ = 9 Hz, 1H, C_2H_4), 1.93 (dd, $^{3}J_{HH}$ = 9 Hz, 1H, C_2H_4). $^{13}C\{^{1}H\}$ NMR (201 MHz, CD_2Cl_2): δ 158.4, 155.1, 150.2, 149.3 (dd, $^{1}J_{FC}$ = 250 Hz, $^{2}J_{FC}$ = 14 Hz, *C*–F), 147.7 (dd, $^{1}J_{FC}$ = 244 Hz, $^{2}J_{FC}$ = 15 Hz, *C*–F), 147.0, 143.6, 140.0, 138.0, 135.1, 132.1, 131.5, 130.4, 129.9, 128.6, 128.5, 127.7, 126.3, 123.2, 122.4, 119.1 (d, $^{3}J_{FC}$ = 21 Hz, carbon 7 or 7'), 116.7 (d, $^{4}J_{FC}$ = 8 Hz), 84.7 (d, $^{4}J_{FC}$ = 8 Hz), 84.4 (d, $^{3}J_{FC}$ = 21 Hz, carbon 7 or 7'), 35.0, 22.0. ^{19}F NMR (564 MHz, CD_2Cl_2): δ -139.7 (ddd, $^{3}J_{FF}$ = 19 Hz, $^{3}J_{HF}$ = 11 Hz, $^{4}J_{HF}$ = 8 Hz), -147.4 (ddd, $^{3}J_{FF}$ = 19, $^{3}J_{HF}$ = 11 Hz, $^{4}J_{HF}$ = 8 Hz). Anal. Calcd. for $C_{26}H_{18}N_2ClF_2Ir$: C, 50.04; H, 2.91; N, 4.49. Found: C, 49.54; H, 2.74; N, 4.24.

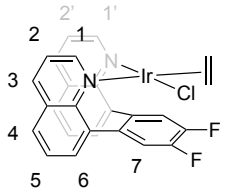

(6-FP)Ir(C_2H_4)(OAc) (4i). In a 100 mL round bottom flask, TlOAc (13.4 mg, 51 μmol) was added to a THF (30 mL) solution of (6-FP)Ir(C_2H_4)Cl (**4h**; 30.0 mg, 51 μmol). The reaction mixture was allowed to stir for 12 h and then filtered through a Celite-loaded fine porosity frit. THF was removed under vacuum. The resulting solid was dissolved in 2 mL of methylene chloride, and then 50 mL of *n*-pentane were added to give a red precipitate. The solid was dried under reduced pressure and collected to give an 85% isolated yield (28.0 mg). See below for structure and assignments. ^{1}H NMR (600 MHz, CD_2Cl_2): δ 10.04 (dd, $^{3}J_{HH}$ = 5 Hz, $^{4}J_{HH}$ = 1 Hz, 1H, *1* or *1*' position), 8.13 – 8.07 (m, 2H, *3* or *3*', *4*, *4*', *5*, *5*', *6* or *6*' position), 7.71 (dd, $^{3}J_{HH}$ = 5 Hz, $^{4}J_{HH}$ = 2 Hz, 1H, *1* or *1*' position), 7.68 (dd, $^{3}J_{HH}$ = 8 Hz, $^{4}J_{HH}$ = 1 Hz, 1H, *3* or *3*' position), 7.46 – 7.41 (m, 3H, *4*, *4*', *5*, *5*', *6* or *6*' position), 7.41 – 7.36 (m, 2H, *2* or *2*', *7* or *7*' position), 7.17 (dd, $^{3}J_{HH}$ = 7, 8 Hz, 1H, *8* or *8*' position), 7.06 (d, $^{3}J_{HH}$ = 8 Hz, 1H, *4*, *4*', *6* or *6*' position), 7.03 (dd, $^{3}J_{HH}$ = 7, $^{4}J_{HH}$ = 2 Hz, 1H, *4*, *4*', *6* or *6*' position), 6.92 (dd, $^{3}J_{HH}$ = 8, 7 Hz, 1H, *8* or *8*' position), 6.83 (d, $^{3}J_{HH}$ = 8 Hz, 1H, *7* or *7*' position), 6.66 (dd, $^{3}J_{HH}$ = 8, 5 Hz, 1H, *2* or *2*' position), 2.83 (dd, $^{3}J_{HH}$ =

10, 9 Hz, 1H, C_2H_4), 2.19 (dd, $^3J_{HH}$ = 10, 8 Hz, 1H, C_2H_4), 1.94 (dd, $^3J_{HH}$ = 9, 9 Hz, 1H, C_2H_4), 1.79 (dd, $^3J_{HH}$ = 9, 9 Hz, 1H, C_2H_4), 1.61 (s, 3H, COCH_3). $^{13}C\{^1H\}$ NMR (201 MHz, CD_2Cl_2): δ 177.6, 157.8, 156.5, 153.1, 152.2, 146.2, 142.9, 135.7, 133.7, 133.4, 132.0, 131.6, 130.1, 129.3, 128.5, 126.9, 126.5, 126.0, 124.6, 123.0, 122.9, 122.0, 110.3, 93.1, 29.2 (C_2H_4), 25.6 (CH_3), 20.1 (C_2H_4). The carbons of ethylene and methyl are distinguished through the H–H and H–C coupling in the HSQC spectrum (Figure S56). Anal. Calcd. for $C_{28}H_{23}N_2IrO_4$: C, 52.24; H, 3.60; N, 4.35. Found: C, 52.28; H, 3.72; N, 4.23.

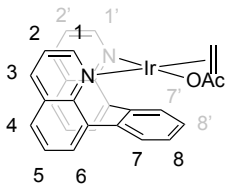

(6-FP)Ir(C_2H_4)(TFA) (4j). In a round bottom flask, a THF (10 mL) solution of 6-FP (30.1 mg, 91 μmol) was added dropwise to a THF (20 mL) solution of $[Ir(COE)_2(\mu\text{-TFA})]_2$ (48.2 mg, 46 μmol). The reaction mixture was allowed to stir overnight, during which time the orange solution turned dark red. The solution was concentrated to ~10 mL in vacuo and transferred to a Fisher Porter reactor. The reactor was sealed, brought out of the glovebox and charged with 50 psig of C_2H_4. The reaction mixture was stirred overnight. Ethylene was released to maintain an approximate 1 atm pressure in the reactor, and the reactor was returned to the glovebox. The reactor was opened in the glovebox, and 50 mL of cold *n*-pentane were added to precipitate a red solid. The mixture was filtered through a fine porosity frit, and the red solid was washed with *n*-pentane and dried under vacuum. Note: the red filtrate can be used to collect additional batches of product using the same procedure. The isolated yield of the first batch was 32% (19.4 mg). See below for structure and assignments. ^1H NMR (600 MHz, CD_2Cl_2): δ 9.95 (dd, $^3J_{HH}$ = 5 Hz, $^4J_{HH}$ = 2 Hz, 1H, *1* or *1*'), 8.14 – 8.13 (m, 2H, *1* or *1*', *4*, *4*', *6* or *6*'), 7.74 – 7.69 (m, 2H, *3* and *3*'), 7.52 – 7.40 (m, 5H, *4*, *4*', *5*, 7 – 7.07 (m, 2H, *7* or *7*', *8* or *8*'), 6.92 (dd, $^3J_{HH}$ = 8 Hz, 1H, *7* or *7*'), 6.87 –

6.82 (m, 1H, *2* or *2*'), 6.70 (dd, $^{3}J_{HH}$ = 8, 5 Hz, 1H, *2* or *2*'), 2.73 (ddd, $^{3}J_{HH}$ = 11, 9 Hz, $^{2}J_{HH}$ = 2 Hz, 1H, C_2H_4), 2.27 (ddd, $^{3}J_{HH}$ = 9, 9 Hz, $^{2}J_{HH}$ = 2 Hz, 1H, C_2H_4), 2.06 (ddd, $^{3}J_{HH}$ = 10, 8 Hz, $^{2}J_{HH}$ = 2 Hz, 1H, C_2H_4), 1.87 (ddd, $^{3}J_{HH}$ = 10, 8 Hz, $^{2}J_{HH}$ = 2 Hz, 1H, C_2H_4). $^{13}C\{^{1}H\}$ NMR (201 MHz, CD_2Cl_2): δ 163.0 (q, $^{2}J_{CF}$ = 35 Hz, $COCF_3$), 157.7, 156.4, 152.9 (two carbons), 145.2, 142.2, 136.4, 134.4, 132.9, 132.4, 132.0, 130.2, 129.3, 128.67, 127.1, 126.9, 126.3, 125.0, 124.4, 122.97, 122.9, 122.1, 113.8 (q, $^{1}J_{CF}$ = 292 Hz, $COCF_3$), 112.3, 95.9, 28.7 (C_2H_4), 19.9 (C_2H_4). ^{19}F NMR (564 MHz, CD_2Cl_2): δ -73.9. Anal. Calcd. for $C_{28}H_{20}N_2IrO_2F_3$: C, 50.52; H, 3.03; N, 4.21. Found: C, 50.71; H, 3.04; N, 4.14.

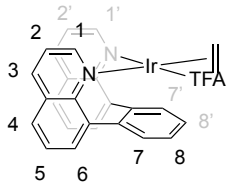

Variable Temperature NMR Study of Rotation of Ethylene. The rotational barriers of the ethylene ligand in "capping arene" ligated Rh and Ir complexes were measured using NMR spectroscopy. For complexes whose ethylene peaks were well-resolved or slightly broadened at room temperature in the ^{1}H NMR spectra, the material was dissolved in DMF-d_7 to prepare an ~0.01 M solution. The spectra were taken at room temperature or lower temperature to record the initial chemical shifts of ethylene resonances. The sample temperature of NMR instrument was then increased, and a spectrum was acquired at intervals of ~10 °C. After the peaks started to broaden, the ^{1}H NMR spectra were acquired at 5 °C intervals. The experiment is complete when 1) the sample temperature has reached 145 °C, 2) the starting complex decomposed, or 3) the ethylene peaks have achieved coalescence and appear sharp again. The temperature was then return to 25 °C to take another spectrum of the complex. Data were assessed for those complexes that returned to their original spectrum after cooling the solution back to 25 °C. Details are in the Supporting Information.

Computational Methods All Density Functional Theory calculations were performed using the Jaguar v10.9 software from Schrodinger Inc.[62] All structures were optimized using the M06-2X[63] meta-GGA functional by Truhlar with the Grimme-Becke-Johnson D3[64] correction for London dispersion. Ir atoms were treated with the Los Alamos small core effective core potential (pseudopotential thus Rh and Ir each have 17 explicit electrons)[65] while all other atoms were treated with the 6-311G**++ basis set (designated LACV3P**++ in Jaguar).[66] Ultra-fine DFT grids were used. Frequency calculations were performed to confirm stationary points and to predict thermochemical properties. Structure optimizations included solvent effects as described by the PBF implicit solvent model; solvent parameters matching THF were used. Natural Bond Orbital analysis was performed using Jaguar's NBO implementation by Glendening and coworkers.[67]

■ ASSOCIATED CONTENT

Supporting Information

Additional experimental details, NMR spectra of the compounds, crystal structure data, and details of computational studies including x, y and z coordinates.

Accession Codes

CCDC 2064397–2064413 contain the supplementary crystallographic data for this paper. These data can be obtained free of charge from The Cambridge Crystallographic Data Centre via www.ccdc.cam.ac.uk/structures.

AUTHOR INFORMATION

Corresponding Author

T. Brent Gunnoe – Department of Chemistry, University of Virginia, Charlottesville, Virginia 22904, United States; orcid.org/0000-0001-5714-3887; Email: tbg7h@virginia.edu

William A. Goddard III – Materials and Process Simulation Center, California Institute of Technology, Pasadena, California 91125, United States; orcid.org/0000-0003-0097-5716; Email: wag@caltech.edu

Authors

Shunyan Gu – Department of Chemistry, University of Virginia, Charlottesville, Virginia 22904, United States; orcid.org/0000-0002-3625-1042

Ke Zhang – Department of Chemistry, University of Virginia, Charlottesville, Virginia 22904, United States; orcid.org/0000-0001-8090-7179

Diane A. Dickie – Department of Chemistry, University of Virginia, Charlottesville, Virginia 22904, United States; orcid.org/0000-0003-0939-3309

Zoë M. Gehman – Department of Chemistry, University of Virginia, Charlottesville, Virginia 22904, United States; orcid.org/0000-0002-2181-6055

Charles B. Musgrave III – Materials and Process Simulation Center, California Institute of Technology, Pasadena, California 91125, United States; orcid.org/0000-0002-3432-0817

Note

The authors declare no competing financial interest.

ACKNOWLEDGEMENTS

The Gunnoe group acknowledges support from the U.S. National Science Foundation (CHE-1800173).

CBM and WAG received support from ONR (N00014-19-1-2081).

REFERENCES

1. O'Reilly, M. E.; Johnson, S. I.; Nielsen, R. J.; Goddard, W. A.; Gunnoe, T. B., Transition-Metal-Mediated Nucleophilic Aromatic Substitution with Acids. *Organometallics* **2016,** *35*, 2053-2056.
2. O'Reilly, M. E.; Fu, R.; Nielsen, R. J.; Sabat, M.; Goddard, W. A.; Gunnoe, T. B., Long-Range C–H Bond Activation by RhIII-Carboxylates. *J. Am. Chem. Soc.* **2014,** *136*, 14690-14693.
3. Chen, J.; Nielsen, R. J.; Goddard III, W. A.; McKeown, B. A.; Dickie, D. A.; Gunnoe, T. B., Catalytic Synthesis of Superlinear Alkenyl Arenes Using a Rh(I) Catalyst Supported by a "Capping Arene" Ligand: Access to Aerobic Catalysis. *J. Am. Chem. Soc.* **2018,** *140*, 17007-17018.
4. Fu, R.; O'Reilly, M. E.; Nielsen, R. J.; Goddard III, W. A.; Gunnoe, T. B., Rhodium Bis(quinolinyl)benzene Complexes for Methane Activation and Functionalization. *Chem. Eur. J.* **2015,** *21*, 1286-1293.
5. Gu, S.; Chen, J.; Musgrave, C. B.; Gehman, Z. M.; Habgood, L. G.; Jia, X.; Dickie, D. A.; Goddard, W. A.; Gunnoe, T. B., Functionalization of Rh^{III}–Me Bonds: Use of "Capping Arene" Ligands to Facilitate Me–X Reductive Elimination. *Organometallics* **2021**, *40*, 1889-1906.
6. Rourke, J., Christoph Elschenbroich. Organometallics. Wiley-VCH, 2006, 3rd edn, p. 818.
7. Keith, J. A.; Henry, P. M., The Mechanism of the Wacker Reaction: A Tale of Two Hydroxypalladations. *Angew. Chem. Int. Ed.* **2009,** *48*, 9038-9049.
8. Ziegler-Natta Catalysts. In *Kirk‐Othmer Encyclopedia of Chemical Technology*, pp 1-22.
9. Grubbs, R. H.; Burk, P. L.; Carr, D. D., Mechanism of the olefin metathesis reaction. *J. Am. Chem. Soc.* **1975,** *97*, 3265-3267.
10. Crabtree, R., Iridium compounds in catalysis. *Acc. Chem. Res.* **1979,** *12*, 331-337.
11. Ittel, S. D.; Johnson, L. K.; Brookhart, M., Late-Metal Catalysts for Ethylene Homo- and Copolymerization. *Chem. Rev.* **2000,** *100*, 1169-1204.
12. de Bruin, B.; Budzelaar, P. H. M.; Gal, A. W., Functional Models for Rhodium-Mediated Olefin-Oxygenation Catalysis. *Angew. Chem. Int. Ed.* **2004,** *43*, 4142-4157.
13. Bennett, M. A., Olefin and Acetylene Complexes of Transition Metals. *Chem. Rev.* **1962,** *62*, 611-652.
14. Dempsey, J. N.; Baenziger, N. C., The Crystal Structure of an Ethylene-Palladium Chloride Complex. *J. Am. Chem. Soc.* **1955,** *77*, 4984-4987.
15. Liu, Z.; Yamamichi, H.; Madrahimov, S. T.; Hartwig, J. F., Rhodium Phosphine−π-Arene Intermediates in the Hydroamination of Alkenes. *J. Am. Chem. Soc.* **2011,** *133*, 2772-2782.
16. Dias, E. L.; Brookhart, M.; White, P. S., Stable, Cationic Alkyl−Olefin Complexes of Ruthenium(II) and Rhodium(III): Effects of Ligand Geometry upon Olefin Insertion/Alkyl Migration. *Organometallics* **2000,** *19*, 4995-5004.
17. Beller, M.; Trauthwein, H.; Eichberger, M.; Breindl, C.; Herwig, J.; Müller, T. E.; Thiel, O. R.,

The First Rhodium-Catalyzed Anti-Markovnikov Hydroamination: Studies on Hydroamination and Oxidative Amination of Aromatic Olefins. *Chem. Eur. J.* **1999,** *5*, 1306-1319.
18. del Río, M. P.; Abril, P.; López, J. A.; Sodupe, M.; Lledós, A.; Ciriano, M. A.; Tejel, C., Activating a Peroxo Ligand for C−O Bond Formation. *Angew. Chem. Int. Ed.* **2019,** *58*, 3037-3041.
19. de Bruin, B.; Boerakker, M. J.; de Gelder, R.; Smits, J. M. M.; Gal, A. W., Amidation of [RhI(ethene)]+ via a 2-Rhodaoxetane. *Angew. Chem. Int. Ed.* **1999,** *38*, 219-222.
20. Feller, M.; Ben-Ari, E.; Diskin-Posner, Y.; Carmieli, R.; Weiner, L.; Milstein, D., O_2 Activation by Metal–Ligand Cooperation with IrI PNP Pincer Complexes. *J. Am. Chem. Soc.* **2015,** *137*, 4634-4637.
21. Liebov, N. S.; Zhu, W.; Chen, J.; Webster-Gardiner, M. S.; Schinski, W. L.; Gunnoe, T. B., Rhodium-Catalyzed Alkenylation of Toluene Using 1-Pentene: Regioselectivity To Generate Precursors for Bicyclic Compounds. *Organometallics* **2019,** *38*, 3860-3870.
22. Zhu, W.; Gunnoe, T. B., Advances in Rhodium-Catalyzed Oxidative Arene Alkenylation. *Acc. Chem. Res.* **2020,** *53*, 920-936.
23. Zhu, W.; Luo, Z.; Chen, J.; Liu, C.; Yang, L.; Dickie, D. A.; Liu, N.; Zhang, S.; Davis, R. J.; Gunnoe, T. B., Mechanistic Studies of Single-Step Styrene Production Catalyzed by Rh Complexes with Diimine Ligands: An Evaluation of the Role of Ligands and Induction Period. *ACS Catal.* **2019,** *9*, 7457-7475.
24. Webster-Gardiner, M. S.; Chen, J.; Vaughan, B. A.; McKeown, B. A.; Schinski, W.; Gunnoe, T. B., Catalytic Synthesis of “Super” Linear Alkenyl Arenes Using an Easily Prepared Rh(I) Catalyst. *J. Am. Chem. Soc.* **2017,** *139*, 5474-5480.
25. Vaughan, B. A.; Khani, S. K.; Gary, J. B.; Kammert, J. D.; Webster-Gardiner, M. S.; McKeown, B. A.; Davis, R. J.; Cundari, T. R.; Gunnoe, T. B., Mechanistic Studies of Single-Step Styrene Production Using a Rhodium(I) Catalyst. *J. Am. Chem. Soc.* **2017,** *139*, 1485-1498.
26. Vaughan, B. A.; Webster-Gardiner, M. S.; Cundari, T. R.; Gunnoe, T. B., A rhodium catalyst for single-step styrene production from benzene and ethylene. *Science* **2015,** *348* (6233), 421-424.
27. Qiu, Y.; Kong, W.-J.; Struwe, J.; Sauermann, N.; Rogge, T.; Scheremetjew, A.; Ackermann, L., Electrooxidative Rhodium-Catalyzed C−H/C−H Activation: Electricity as Oxidant for Cross-Dehydrogenative Alkenylation. *Angew. Chem. Int. Ed.* **2018,** *57*, 5828-5832.
28. Ackermann, L., Carboxylate-Assisted Transition-Metal-Catalyzed C−H Bond Functionalizations: Mechanism and Scope. *Chem. Rev.* **2011,** *111*, 1315-1345.
29. Choi, J.; MacArthur, A. H. R.; Brookhart, M.; Goldman, A. S., Dehydrogenation and Related Reactions Catalyzed by Iridium Pincer Complexes. *Chem. Rev.* **2011,** *111*, 1761-1779.
30. Kim, J. Y.; Park, S. H.; Ryu, J.; Cho, S. H.; Kim, S. H.; Chang, S., Rhodium-Catalyzed Intermolecular Amidation of Arenes with Sulfonyl Azides via Chelation-Assisted C–H Bond Activation. *J. Am. Chem. Soc.* **2012,** *134*, 9110-9113.
31. Park, S. H.; Kim, J. Y.; Chang, S., Rhodium-Catalyzed Selective Olefination of Arene Esters via C−H Bond Activation. *Org. Lett.* **2011,** *13*, 2372-2375.
32. Jones, W. D.; Feher, F. J., Comparative reactivities of hydrocarbon carbon-hydrogen bonds with a transition-metal complex. *Acc. Chem. Res.* **1989,** *22*, 91-100.
33. Zhao, S.-B.; Song, D.; Jia, W.-L.; Wang, S., Regioselective C−H Activation of Toluene with a 1,2-Bis(N-7-azaindolyl)benzene Platinum(II) Complex. *Organometallics* **2005,** *24*, 3290-3296.
34. Tan, R.; Jia, P.; Rao, Y.; Jia, W.; Hadzovic, A.; Yu, Q.; Li, X.; Song, D., Diplatinum Complexes Supported by Novel Tetradentate Ligands with Quinoline Functionalities for Tandem C−Cl

Activation and Dearomatization. *Organometallics* **2008,** *27*, 6614-6622.
35. Bianchi, F.; Gallazzi, M. C.; Porri, L.; Diversi, P., Disproportionation of the cyclooctene ligand in the reaction of $[IrCl(C_8H_{14})_2]_2$ with $AgOCOCF_3$: formation of $[Ir(OCOCF_3)(C_8H_{14})_2]_2$ and $[Ir(OCOCF_3)(1,5\text{-}C_8H_{12}]_2$ and their conversion into cationic arene complexes. *J. Organomet. Chem.* **1980,** *202* (1), 99-105.
36. Kumar, A.; Bhatti, T. M.; Goldman, A. S., Dehydrogenation of Alkanes and Aliphatic Groups by Pincer-Ligated Metal Complexes. *Chem. Rev.* **2017,** *117*, 12357-12384.
37. Dobereiner, G. E.; Crabtree, R. H., Dehydrogenation as a Substrate-Activating Strategy in Homogeneous Transition-Metal Catalysis. *Chemical Reviews* **2010,** *110*, 681-703.
38. Moseley, K.; Kang, J. W.; Maitlis, P. M., Pentamethylcyclopentadienyl-rhodium and -iridium halides. Part II. Reactions with mono-, di-, and tri-olefins. *J. Chem. Soc. A. Inorg. Phys. Theor.* **1970,** 2875-2883.
39. Based on the results from the Cambridge Structural Database
40. Gunnoe, T. B.; Sabat, M.; Harman, W. D., Enantiofacial Discrimination in Dihapto-Coordination of Aromatic Molecules by the Chiral π-Base/σ-Lewis Acid {$TpRe(CO)(PMe_3)$}. *J. Am. Chem. Soc.* **1999,** *121*, 6499-6500.
41. Valahovic, M. T.; Gunnoe, T. B.; Sabat, M.; Harman, W. D., Ligand-Modulated Stereo- and Regioselective Tandem Addition Reactions of Rhenium-Bound Naphthalene. *J. Am. Chem. Soc.* **2002,** *124*, 3309-3315.
42. Gunnoe, T. B.; Sabat, M.; Harman, W. D., Reactions of $TpRe(CO)_2(THF)$ with Aromatic Molecules (Tp = Hydridotris(pyrazolyl)borate). *J. Am. Chem. Soc.* **1998,** *120*, 8747-8754.
43. Physical Methods. In *The Organometallic Chemistry of the Transition Metals*, pp 259-289.
44. Galindo, A.; Pastor, A.; Perez, P. J.; Carmona, E., Bis(ethylene) complexes of molybdenum and tungsten and their reactivity toward carbon dioxide. New examples of acrylate formation by coupling of ethylene and carbon dioxide. *Organometallics* **1993,** *12*, 4443-4451.
45. Pell, C. J.; Zhu, Y.; Huacuja, R.; Herbert, D. E.; Hughes, R. P.; Ozerov, O. V., Fluorocarbene, fluoroolefin, and fluorocarbyne complexes of Rh. *Chem. Sci.* **2017,** *8*, 3178-3186.
46. Cramer, R., Olefin Coordination Compounds of Rhodium: The Barrier to Rotation of Coordinated Ethylene and the Mechanism of Olefin Exchange. *J. Am. Chem. Soc.* **1964,** *86*, 217-222.
47. Cramer, R.; Kline, J. B.; Roberts, J. D., Bond character and conformational equilibration of ethylene- and tetrafluoroethylenerhodium complexes from nuclear magnetic resonance spectra. *J. Am. Chem. Soc.* **1969,** *91*, 2519-2524.
48. Adams, J. J.; Arulsamy, N.; Roddick, D. M., An investigation of ethylene rotational barriers for 5-coordinate d8 metal bis-ethylene complexes. *Polyhedron* **2014,** *84*, 209-215.
49. Werner, H.; Ortmann, D. A.; Gevert, O., Novel trialkylstibane iridium(I) and iridium(III) complexes including the x-ray crystal structure of five-Coordinate $[IrCl(C_2H_4)_2(SbiPr_3)_2]$. *Chemische Berichte* **1996,** *129*, 411-417.
50. Lundquist, E. G.; Huffman, J. C.; Folting, K.; Caulton, K. G., Mechanism of Ethylene Hydrogenation by the Molecular Hydrogen Complex $[Ir(H)_2(H_2)(PMe_2Ph)_3]^+$ — Characterization of Intermediates. *Angew. Chem. Int. Ed.* **1988,** *27*, 1165-1167.
51. Aizenberg, M.; Milstein, D.; Tulip, T. H., Isolation, Characterization, and Interconversions of $(Et_3P)_2Ir(C_2H_4)_nCl$ (n = 1, 2). *Organometallics* **1996,** *15*, 4093-4095.
52. Kiel, G. Y.; Takats, J.; Grevels, F. W., Multisubstitution of $Os(CO)_5$ by ethylene: isomeric $Os(CO)_2(C_2H_4)_3$ and a derivative of $Os(CO)(C_2H_4)_4$. *J. Am. Chem. Soc.* **1987,** *109*, 2227-2229.

53. Adams, J. J.; Arulsamy, N.; Roddick, D. M., Acceptor PCP Pincer Iridium(I) Chemistry: Stabilization of Nonmeridional PCP Coordination Geometries. *Organometallics* **2011,** *30*, 697-711.
54. Lundquist, E. G.; Folting, K.; Streib, W. E.; Huffman, J. C.; Eisenstein, O.; Caulton, K. G., Reactivity of the molecular hydrogen complex $[IrH_4(PMe_2Ph)_3]BF_4$ towards olefins. The origin of stereochemical rigidity of $M(PR_3)_3(olefin)_2$ species. *J. Am. Chem. Soc.* **1990,** *112*, 855-863.
55. Rossi, A. R.; Hoffmann, R., Transition metal pentacoordination. *Inorg. Chem.* **1975,** *14*, 365-374.
56. Kim, C. K.; Lee, K. A.; Kim, C. K.; Lee, B.-S.; Lee, H. W., NBO analyses of the back-bonding in metal–olefin complexes. *Chem. Phys. Lett.* **2004,** *391*, 321-324.
57. Rauk, A., *Orbital Interaction Theory of Organic Chemistry*. Wiley: New York, 2001; p 37.
58. Ammann, C.; Meier, P.; Merbach, A. E., A simple multinuclear NMR thermometer. *J. Magn. Reson.* **1982,** *46*, 319-321.
59. Onderdelinden, A. L.; van der Ent, A., Chloro- and bromo-(alkene)iridium(I) complexes. *Inorg. Chim. Acta* **1972,** *6*, 420-426.
60. Arthurs, M. A.; Bickerton, J.; Stobart, S. R.; Wang, J., Pyrazolyl-Bridged Iridium Dimers. 17.1 Tetrakis(alkene)diiridium(I) Complexes: $[Ir(\eta^2\text{-}C_2H_4)_2(\mu\text{-}Cl)]_2$ as a Precursor to $[Ir(\eta^2\text{-}C_2H_4)_2(\mu\text{-}pz)]_2$. Stereochemically Nonrigid Behavior of the Analogue $[Ir(\eta^2\text{-}C_2H_4)(\eta^2\text{-}C_2F_4)(\mu\text{-}Cl)]_2$. *Organometallics* **1998,** *17*, 2743-2750.
61. Cramer, R.; McCleverty, J. A.; Bray, J., Di-μ-chlorotetrakis(ethylene)dirhodium(I), 2,4-Pentanedionatobis(ethylene)rhodium(I), and Di-μ-chlorotetracarbonyldirhodium(I). In *Inorg. Synth.*, Parshall, G. W., Ed. 1974.
62. Bochevarov, A. D.; Harder, E.; Hughes, T. F.; Greenwood, J. R.; Braden, D. A.; Philipp, D. M.; Rinaldo, D.; Halls, M. D.; Zhang, J.; Friesner, R. A., Jaguar: A high-performance quantum chemistry software program with strengths in life and materials sciences. *International Journal of Quantum Chemistry* **2013,** *113*, 2110-2142.
63. Wang, Y.; Verma, P.; Jin, X.; Truhlar, D. G.; He, X., Revised M06 density functional for main-group and transition-metal chemistry. *Proc. Nat. Acad. Sci.* **2018,** *115*, 10257.
64. Grimme, S.; Ehrlich, S.; Goerigk, L., Effect of the damping function in dispersion corrected density functional theory. *J. Comp. Chem.* **2011,** *32* (7), 1456-1465.
65. Roy, L. E.; Hay, P. J.; Martin, R. L., Revised Basis Sets for the LANL Effective Core Potentials. *Journal of Chemical Theory and Computation* **2008,** *4* (7), 1029-1031.
66. Krishnan, R.; Binkley, J. S.; Seeger, R.; Pople, J. A., Self‐consistent molecular orbital methods. A basis set for correlated wave functions. *J. Chem. Phys.* **1980,** *72*, 650-654.
67. Glendening, E. D.; Weinhold, F., Natural resonance theory: I. General formalism. *J. Comp. Chem.* **1998,** *19*, 593-609.

TOC Graphic

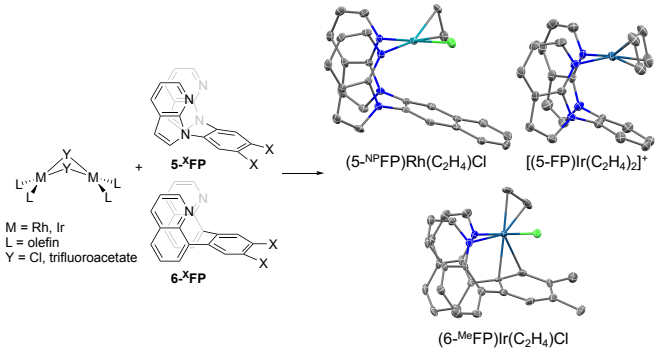
M = Rh, Ir
L = olefin
Y = Cl, trifluoroacetate
5-XFP
6-XFP
(5-NPFP)Rh(C2H4)Cl
[(5-FP)Ir(C2H4)2]+
(6-MeFP)Ir(C2H4)Cl